Master Thesis

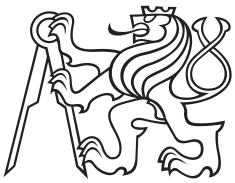

Czech Technical University in Prague

F3

Faculty of Electrical Engineering
Department of Control Engineering

Active torque vectoring systems for electric drive vehicles

Martin Mondek

Supervisor: doc. Ing. Martin Hromčík, Ph.D.
Field of study: Cybernetics and robotics
Subfield: Systems and control
January 2018

ZADÁNÍ DIPLOMOVÉ PRÁCE

I. OSOBNÍ A STUDIJNÍ ÚDAJE

Příjmení: **Mondek** Jméno: **Martin** Osobní číslo: **406357**

Fakulta/ústav: **Fakulta elektrotechnická**

Zadávající katedra/ústav: **Katedra řídicí techniky**

Studijní program: **Kybernetika a robotika**

Studijní obor: **Systémy a řízení**

II. ÚDAJE K DIPLOMOVÉ PRÁCI

Název diplomové práce:

Systémy aktivního řízení momentu pro elektromobily

Název diplomové práce anglicky:

Active torque vectoring systems for electric drive vehicles

Pokyny pro vypracování:

Cílem práce je navrhnout a zvalidovat vybrané zákony řízení pro systém vektorování momentu elektricky poháněného automobilu. Návrh algoritmů řízení založte na zjednodušeném modelu stranové dynamiky pomocí vybraných klasických a moderních metod. Ověření všech navržených řešení proveďte simulačně a vybrané úlohy zvalidujte i experimentálně.
1. Seznamte se s problematikou elektrických automobilů a jejich řízení.
2. Vyberte vhodný model pneumatiky a vytvořte jednostopý dynamický model vozidla.
3. Model linearizujte a proveďte lineární analýzu tohoto systému.
4. Na základě analýzy navrhněte jednoduché zákony řízení a proveďte jejich simulační validaci a verifikaci.
5. Vytvořené algoritmy řízení aplikujte na vozidle poskytnutém firmou Porsche Engineering Services s.r.o.

Seznam doporučené literatury:

[1] VLK, František. Dynamika motorových vozidel. 2. vyd. Brno: František Vlk, 2003. ISBN 80-239-0024-2.
[2] SCHRAMM, Dieter, Roberto BARDINI a Manfred HILLER. Vehicle Dynamics: Modeling and Simulation. Heidelberg: Springer, 2014. ISBN
978-3-540-36044-5.
[3] JAZAR, Reza N. Vehicle dynamics: theory and application. 2nd ed. New York: Springer, c2014. ISBN 978-1-4614-8543-8.

Jméno a pracoviště vedoucí(ho) diplomové práce:

doc. Ing. Martin Hromčík, Ph.D., katedra řídicí techniky FEL

Jméno a pracoviště druhé(ho) vedoucí(ho) nebo konzultanta(ky) diplomové práce:

Datum zadání diplomové práce: **08.02.2017** Termín odevzdání diplomové práce: **09.01.2018**

Platnost zadání diplomové práce: **30.09.2018**

doc. Ing. Martin Hromčík, Ph.D.	prof. Ing. Michael Šebek, DrSc.	prof. Ing. Pavel Ripka, CSc.
podpis vedoucí(ho) práce	podpis vedoucí(ho) ústavu/katedry	podpis děkana(ky)

III. PŘEVZETÍ ZADÁNÍ

Diplomant bere na vědomí, že je povinen vypracovat diplomovou práci samostatně, bez cizí pomoci, s výjimkou poskytnutých konzultací. Seznam použité literatury, jiných pramenů a jmen konzultantů je třeba uvést v diplomové práci.

. | Podpis studenta

Datum převzetí zadání

Acknowledgements

I would like to thank my supervisor doc. Ing. Martin Hromčík, Ph.D. for his valuable advice and guidance during the creation of this thesis.

Great thanks also belong to all employees and representatives of the Porsche Engineering Services s.r.o. for very helpful consultations and for providing the experimental vehicle. I namely thank Ing. Juraj Madaras, Ph.D. for his willingness to participate in experimental tests.

I also thank my parents and friends for support, without which this work would not be completed.

Poděkování

Rád bych poděkoval zejména vedoucímu mé diplomové práce doc. Ing. Martinu Hromčíkovi, Ph.D. za jeho cenné rady v průběhu vytváření této práce.

Velké poděkování také patří všem zaměstnancům a představitelům firmy Porsche Engineering Services s.r.o. za velmi přínosné konzultace a zejména pak za umožnění přístupu k testovacímu vozidlu. Jmenovitě pak děkuji Ing. Juraji Madarasovi, Ph.D. za jeho ochotu podílet se na experimentálních testech.

Dále děkuji mým rodičům a kamarádům za podporu, bez které by vznik této práce nebyl možný.

Declaration

I declare that this thesis was finished on my own and I have specified all sources in the list of references according to the methodical guideline on the observance of ethical principles in the preparation of university graduate thesis.

Prohlášení

Prohlašuji, že jsem předloženou práci vypracoval samostatně a že jsem uvedl veškeré použité informační zdroje v souladu s Metodickým pokynem o dodržování etických principů při přípravě vysokoškolských závěrečných prací.

In Prague/V Praze, 9. 1. 2018

Abstract

Various torque vectoring systems for an electric vehicle are presented and discussed in this thesis. Several vehicle mathematical models for simulations of the vehicle dynamics or the development of the control systems are introduced. Effects of variations in the physical parameters of the vehicle models on the response times, damping ratios, natural frequencies and other dynamical characteristics are described. Presented vehicle models were parameterized to match the behavior of the real test vehicle. The developed torque vectoring control systems are implemented to the professional automotive control software, and their performance is tested in various experiments. Finally, the results of all tests of vehicle dynamics are compared and evaluated.

Keywords:
vehicle dynamics, vehicle stability, electric vehicles, control systems, torque vectoring system, oversteer, understeer, vehicle dynamics experiments

Supervisor:
doc. Ing. Martin Hromčík, Ph.D.
České vysoké učení technické
v Praze,
Fakulta elektrotechnická,
Katedra řídicí techniky - K13135,
Karlovo náměstí 13,
12135 Praha 2

Abstrakt

V této práci jsou prezentovány a popsány různé systémy rozdělení hnacího momentu u elektrických vozidel. Je představeno několik matematických modelů vozidel pro simulaci jízdní dynamiky nebo pro vývoj řídících systémů. Dále jsou popsány vlivy změn fyzických parameterů na různé vlastnosti prezentovaných matematických modelů, jako jsou časové odezvy, přirozené frekvence a další dynamické parametry. Prezentované matematické modely byly parametrizovány tak, aby jejich dynamika odpovídala reálnému testovacímu vozidlu. Vyvinuté řídicí systémy pro distribuci momentu byly implementovány do profesionálního softwaru pro řízení automobilů a jejich vlastnosti byly otestovány při různých experimentech. Závěrem diplomové práce jsou prezentovány výsledky testů jízdní dynamiky jednotlivých řídících systémů.

Klíčová slova:
dynamika vozidla, stabilita vozidla, elektrická vozidla, řídící systémy, torque vectoring systém, přetáčivost, nedotáčivost, testy jízdní dynamiky

Překlad názvu:
Systémy aktivního řízení momentu pro elektromobily

Contents

1 Introduction **1**

1.1 Assistance systems 2

1.2 Torque vectoring system . . . 3

2 The vehicle modelling **7**

2.1 Introduction 7

2.2 Tire models 7

2.2.1 Pacejka's 'Magic' formula 10

2.2.2 Linear and two-lines tire model 11

2.2.3 Tire models comparison 11

2.3 Kinematic vehicle model . . 12

2.4 Single track vehicle model 13

2.5 Linear vehicle model with constant velocity 16

2.5.1 Linear model and with yaw moment as input 17

3 Linear analysis **19**

3.1 Introduction 19

3.2 Vehicle velocity 20

3.3 Position of the centre of gravity 22

3.4 Moment of inertia 26

3.5 Vehicle weight 28

3.6 Additional properties of linear vehicle model 31

3.6.1 Critical speed 31

4 Parameterization and vehicle simulation **35**

4.1 Introduction 35

4.2 Test Vehicle 35

4.3 Vehicle parameters 36

4.3.1 Measurable vehicle parameters 36

4.3.2 Experimentally identified vehicle parameters 37

4.4 Parameter validation 38

4.4.1 Slow speed steer 38

4.4.2 High-speed steer 39

5 Torque vectoring control system **41**

5.1 Introduction 41

5.2 Feedforward control 41

5.3 Feedback control 43

5.3.1 Generator of reference values 43

5.3.2 Feedback control: yaw rate 45

5.3.3 Feedback control: side acceleration 45

5.4 Control systems target integration 46

6 Experimental results **49**

6.1 Introduction 49

6.2 Torque vectoring test maneuvers 49

6.3 Torque vectoring actuator authority experiments 50

6.4 Experimental results of torque vectoring systems 53

6.4.1 Results of feedforward control 53

6.4.2 Results of feedback control: yaw rate 56

6.4.3 Results of feedback control: side acceleration . . 57

7 Results **61**

8 Conclusions and future work **63**

A Bibliography **65**

B List of abbreviations **67**

C List of symbols **69**

Chapter 1

Introduction

The latest spread of the electromobility in the vehicle industry promises to bring mostly the local improvement of the air pollution and lower operating costs of the vehicle. The electromobility brings not only these very often mentioned properties, but also other advantages such as an independent electric motor for each wheel. The different structure of the powertrain in electrical or hybrid vehicle offers new possibilities for independent control of each wheel. These opportunities requires development of better control algorithms for vehicle stabilization or modification of the vehicle dynamics and behavior.

The modelling and simulation of the vehicle dynamics is very wide discipline. The high fidelity dynamics models of the vehicle motion are often used for the simulations of the exact vehicle behavior. However, simplified mathematical models are sufficient for fundamental study of the vehicle dynamics. The comparison of the vehicle mathematical models with evaluation of the data from real test vehicle is one of the goals of this thesis.

The primary goal of this thesis is to develop and confirm main concepts of the torque vectoring and study the influence of different torque moments on the vehicle states. Several basic control concepts are introduced and experimentally tested on the test vehicle provided by Porsche Engineering Services s.r.o.

First, the mathematical vehicle dynamics are derived in chapter 2. Then the linear constant velocity vehicle model is analyzed in chapter 3. In chapter 4 the vehicle parameterization is described and evaluated. Next, the simple torque vectoring systems with implementation are given in chapter 5. The experimental results of presented torque vectoring systems are in chapter 6. The summary of achieved results is presented in chapter 7 and finally conclusion and future work are presented in the chapter 8.

1.1 Assistance systems

Various advanced or straightforward control systems help the casual driver with the vehicle control, stability, and maneuverability. These systems usually increase the passenger's safety or simplify the driver's effort needed for the driving of the vehicle.

The selection and brief characteristics of existing modern vehicle driver's assistance systems are presented in this subsection. Advanced information about the vehicle dynamics control systems can be found in [19].

- **Cruise control** is an automatic system, which controls the vehicle forward velocity. In modern vehicles this system is called adaptive cruise control and the input is usually extended by additional sensors, which provide useful information about the situation in front of the vehicle. This adaptive cruise control system can then adjust the speed or request an emergency braking to avert an accident without any driver's action.

- **Anti-lock braking system** (ABS) is a control system, which helps mainly during the critical weather conditions such as wet or slippery road surface or during other dangerous situations such as an obstacle in the vehicle path. This system prevents the blocking of the wheels and increases the maneuverability of the vehicle during the critical conditions and decreases the probability of the vehicle skid or crash. This system controls the braking fluid pressure during the full break request.

- **Traction control** is a control system, which extends the ABS system. The traction control helps with the critical situations during the vehicle start or acceleration mainly on surfaces with low friction. This system then decreases the drive torque or slows down the slipping wheel using brakes. This control action then helps to keep the vehicle in the specified direction and relieves the driver's workload.

- **Electronic stability program** (ESP) is a control system, which uses the vehicle braking system as the control actuator for vehicle stabilization. This system usually breaks one wheel to achieve higher or lower vehicle yaw rate depending on the vehicle understeer or oversteer behavior. This control action should provide the vehicle stability during all critical situations. An example of the ESP control of the understeer and oversteer vehicles is presented in figure 1.1 and 1.2.

- **Torque vectoring** is described in the section 1.2.

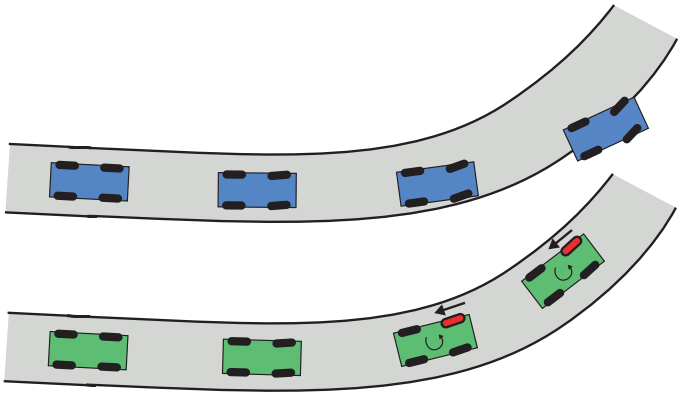

Figure 1.1: The comparison of the understeer vehicle maneuver without and with ESP control systems. The red wheel is slowed down by the control system and creates additional vehicle yaw moment, which stabilizes the vehicle. The term understeer means the tendency of the vehicle to steer less than the driver wants to.

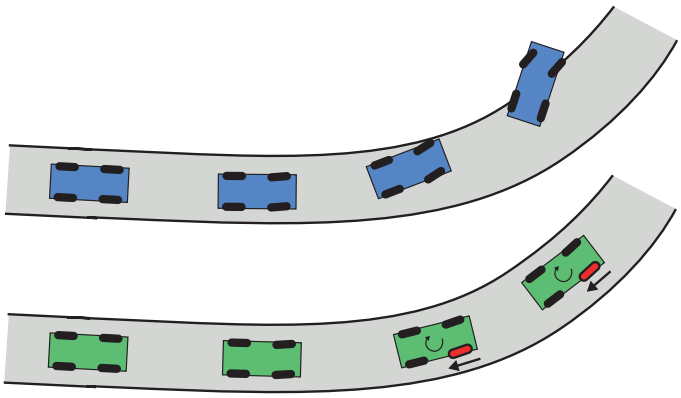

Figure 1.2: The comparison of the oversteer vehicle maneuver without and with ESP control systems. The red wheel is slowed down by the control system and creates additional vehicle yaw moment, which stabilizes the vehicle. The term oversteer means the tendency of the vehicle to steer more than the driver wants to.

1.2 Torque vectoring system

The primary motivation for developing the torque vectoring system is to control the vehicle stability and lateral dynamics, and improve the vehicle maneuverability to lower the driver's effort. All these goals are also goals of the electronic stability system. ESP control system uses breaking of selected wheels to control the vehicle stability, but the torque vectoring system uses the difference of torques for the same purposes.

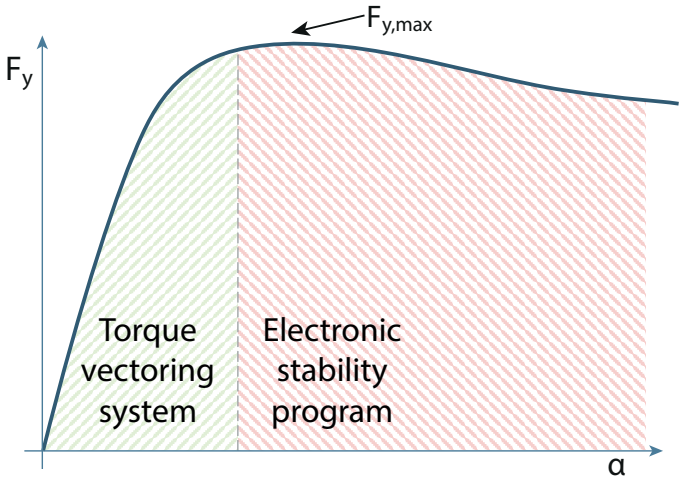

Figure 1.3: Area of lateral sideslip characteristics, where torque vectoring is used to control and modify the vehicle dynamics.

However, the torque vectoring system is used in different situations than the electronic stability program. The torque vectoring system is used to modify the lateral vehicle dynamics, improve the stability and maneuverability of the vehicle.These situations are usually not critical. On the other hand, the electronic stability system controls the vehicle stability in dangerous situations, where some severe damage might be caused. If the ESP system starts to control the vehicle, the torque vectoring system should be turned off.

The comparison of application of the torque vectoring system and an electronic stability system is shown in figure 1.3. The curve expresses the lateral sideslip characteristics of the tire (see section 2.2) and areas of the torque vectoring system and electronic stability program application are displayed.

The vehicle yaw moment is stabilized or agilized by additional yaw moment created by the difference in the vehicle torque distribution. The figure 1.4 displays the difference between rear wheel torque and the generated yaw moment. This yaw moment then forces the vehicle dynamics to turn more, which results to increment of the vehicle yaw rate.

The torque vectoring control action example is presented in figures 1.5 and 1.6. The main difference with the ESP algorithm is the selected controlled wheel (see fig. 1.1 and 1.2).

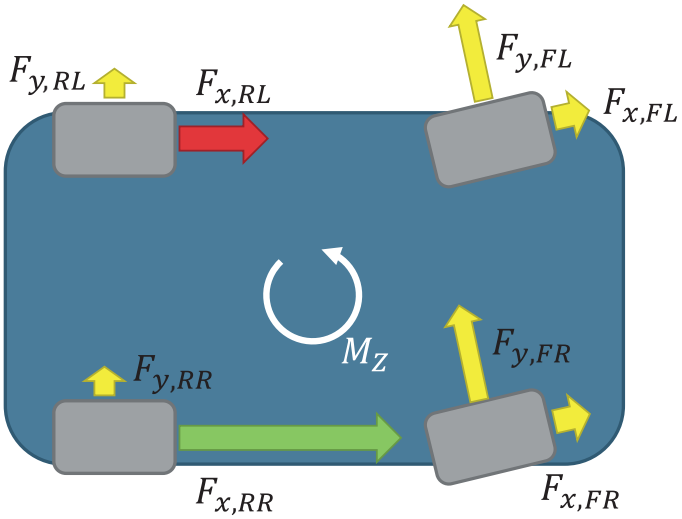

Figure 1.4: The difference in the rear wheel torque creates additional vehicle yaw moment, which can be used for the control of the vehicle stability.

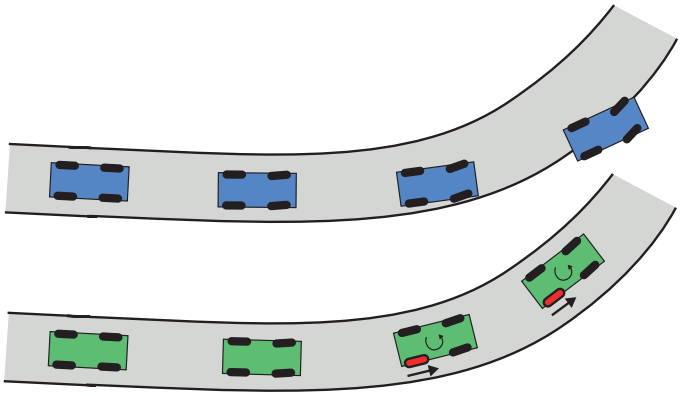

Figure 1.5: The comparison of the understeer vehicle maneuver without and with torque vectoring control system. The control system increases the torque on the wheel with the red color. This action creates additional vehicle yaw moment, which stabilizes the vehicle.

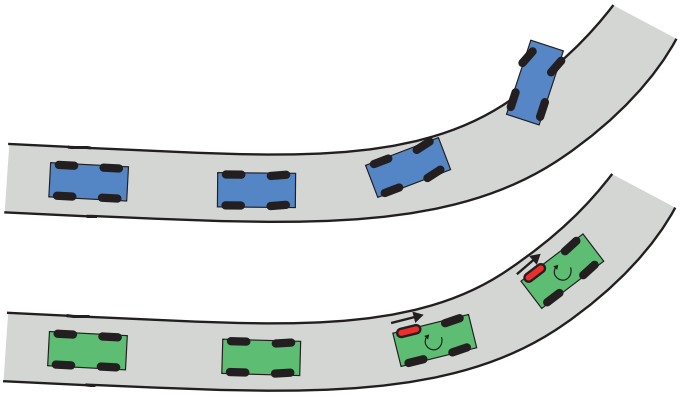

Figure 1.6: The comparison of the oversteer vehicle maneuver without and with torque vectoring control system. The control system increases the torque on the wheel with the red color. This action creates additional vehicle yaw moment, which stabilizes the vehicle.

The theoretical background of the torque vectoring system and its application in various vehicles can be found in [15]. Simple torque vectoring actuator analysis is given in [10]. Various torque vectoring control systems such as simple feedforward control or feedback reference value control or their combination are presented in [2, 7, 6] . These papers use simulation studies for the evaluation of the results. On the other hand, the application on the test vehicle and the experimental results and evaluation of the control systems is the main contribution of this thesis.

Chapter 2

The vehicle modelling

2.1 Introduction

The vehicle dynamics described in this chapter supports the development of control algorithms and simulation, which are described in chapter 5. During the system description, several parts of the vehicle dynamics are simplified. For torque vectoring system development and simulation of the vehicle cornering the planar model of the car is used. Vertical movement together with the roll motion of the vehicle body is omitted.

In this chapter selection of existing tire models is introduced first. Then the kinematic model of the vehicle is described. After that the single track vehicle model is introduced, and finally, this dynamic system is linearized.

2.2 Tire models

The mathematical description of the interaction between the vehicle tire and the road surface is the biggest challenge of models and simulations describing vehicle behavior. Such models can evaluate longitudinal and lateral tire forces using vehicle states as input. For purposes of this thesis minor tire dynamics are neglected such as self-aligning torque, the combined slip, the influence of the camber angle and the tire deflection. Advanced tire characteristics, mathematical models and description of the tire behavior can be found in [14]. Good overview of the tire models is also in [4].

The most significant inputs for later considered tire models are side-slip angle α, longitudinal slip λ and normal load F_z of a particular tire. The

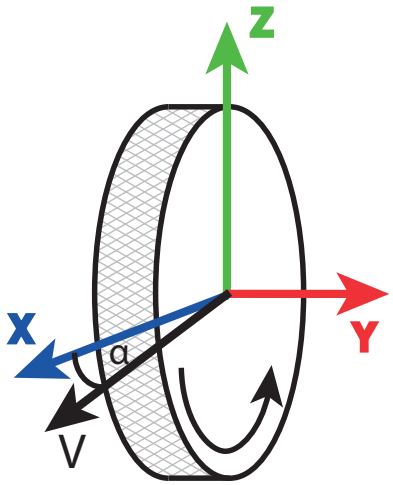

Figure 2.1: Tire coordination system used within this thesis.

side-slip angle α and longitudinal slip λ are defined as follows:

$$\lambda = \left| \frac{v_x - v_c}{v_x} \right|, \tag{2.1}$$

$$\alpha = \arctan\left(\frac{v_y}{v_x}\right), \tag{2.2}$$

where v_c is the circumferential velocity of the tire, v_x is longitudinal velocity of the tire center and v_y is lateral tire velocity of the tire center, both with respect to the ground. (see fig. 2.1)

Longitudinal and lateral forces transferred by the tire and their dependency on the longitudinal slip and side-slip angle respectively, are commonly expressed by the slip curve. The longitudinal acceleration is considered to be zero in this thesis; the vehicle is moving at constant forward speed. Therefore only lateral tire forces and only side-slip angle to a lateral force slip characteristic is considered from now on. The example of this slip curve used in this thesis is presented in 2.2.

The initial slope at zero side-slip angle of the characteristic is called nominal cornering stiffness $C_{\alpha 0}$. For a small side-slip angle α the characteristic is linear and the generated side force F_y is equal to the side-slip value multiplied with this nominal cornering stiffness coefficient. This behavior is used in the linear tire model described in section 2.2.2. However, as the side-slip angle increases, the tire starts to be overloaded and the generated side force is not linear up to the point where the slip curve reaches the maximum of the friction coefficient μ_{max}. With further increase of the side-slip angle, the tire is not able to transfer higher forces F_y.

The typical side-slip curve for lateral motion differs with varying normal load F_z. This trend is shown in figure 2.3. As the normal force increases, the

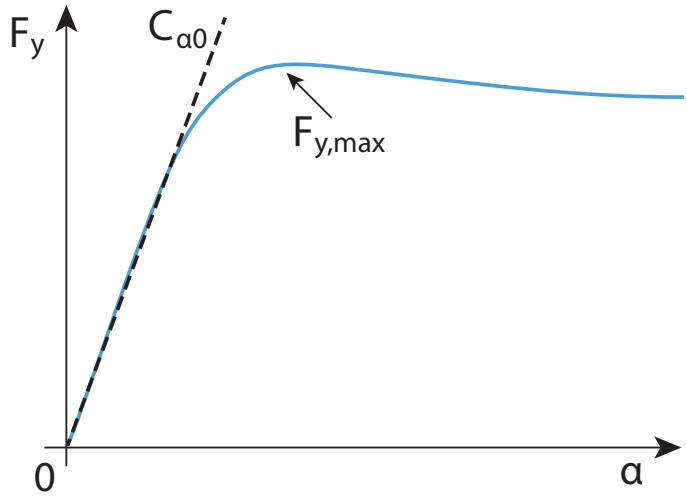

Figure 2.2: An example of typical side-slip characteristics for lateral motion.

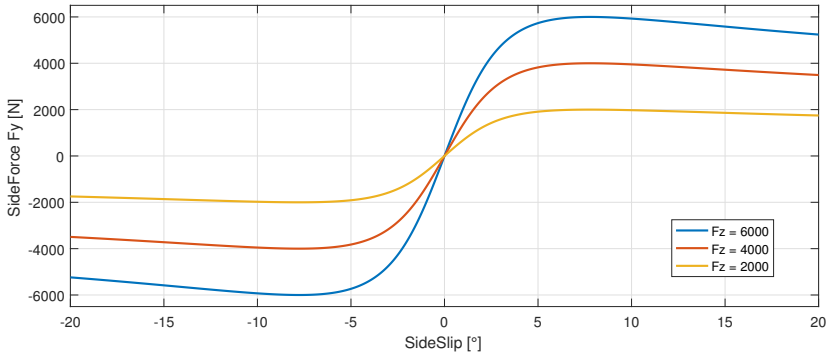

Figure 2.3: Lateral tire characteristics for different normal loads.

maximal transferred side force F_y is also growing. Since the vehicle described within this thesis is a sports car with a very low height of the center of gravity, it is assumed, that normal forces depend only on the weight distribution of the vehicle and that these forces are constant during the vehicle movement. In other words, neither longitudinal nor lateral load transfer is considered in this thesis. The aerodynamic down-force of the vehicle is also neglected for simplification of the model.

The lateral side-slip curve depends not only on tire characteristics, but also on different conditions such as inflation of the tire, surface conditions (eg. dry/wet tarmac, snow, ice), the temperature of the tire or the road. The influence of different surfaces on maximal tire friction coefficient μ_{max} is shown in figure 2.4. The tire friction coefficient can be computed as follows:

$$\mu_{x,max} = \frac{F_{x,max}}{F_z}, \qquad \mu_{y,max} = \frac{F_{y,max}}{F_z}. \tag{2.3}$$

This coefficient in longitudinal direction is close to 1 for dry and clean tarmac.

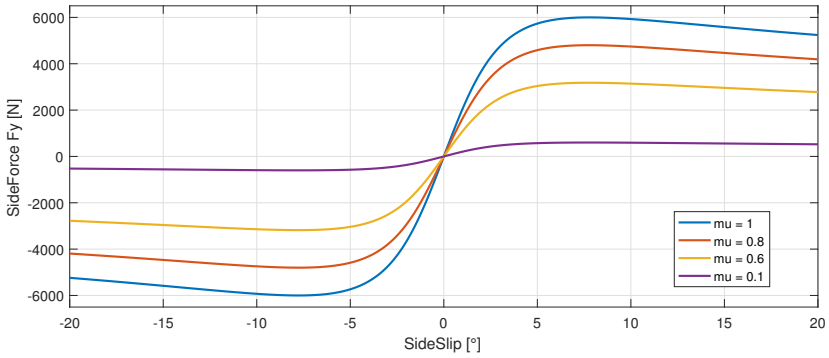

Normal load $F_z = 6000$ N, friction of the road surface corresponds to dry asphalt ($\mu = 1$), wet asphalt ($\mu = 0.8$), snow ($\mu = 0.6$), ice ($\mu = 0.1$).

Figure 2.4: Lateral slip curve for different surfaces.

On wet tarmac we obtain values between 0.8 and 0.9, on snow approximately 0.6 and on ice 0.1.

2.2.1 Pacejka's 'Magic' formula

The original empirical formula of Hans Bastiaan Pacejka [13] considered more than 20 coefficients. It also considers both longitudinal and lateral tire force characteristics, which are computed simultaneously in their mutual interdependence. This set of factors was later reduced to 4 main parameters (B,C,D and E). The approximate value of these main parameters is estimated by fitting the formula to empirical measurements of the tire behavior. On top of that, longitudinal and lateral tire forces can be computed independently for more straightforward implementation and representation of the formula.

The general simplified form of Pacejka's 'Magic' formula is:

$$F_y(\alpha) = D \cdot \sin\left(C \cdot \arctan\left(B\alpha - E(\, B\alpha - \arctan\left(B\alpha\right)\,)\right)\right), \tag{2.4}$$

where parameters B,C,D and E give the shape of the tire characteristics, F_y is lateral tire force and α is side-slip angle of the tire. The same formula (with different empirical parameters) can be used for estimating the longitudinal tire force F_x if the side-slip angle is replaced with slip of the tire λ.

The parameter D is the peak value of the side-slip curve. The parameter C (shape factor) determines the shape around the peak value of the curve. The value B is the stiffness factor. Finally, the value E (curvature factor) determines how much will the shape decline after the maximal transferable lateral force is reached. The computation of the stiffness factor of the tire C_α can be found in equation 2.5.

$$C_\alpha = B \cdot C \cdot D \tag{2.5}$$

2.2.2 Linear and two-lines tire model

The linear model is the simplest model of the tire. It is defined as

$$F_x(\lambda) = C_{\lambda 0}\lambda, \qquad F_y(\alpha) = C_{\alpha 0}\alpha, \tag{2.6}$$

where $C_{\lambda 0}$ is the tire slip coefficient and $C_{\alpha 0}$ is the side-slip coefficient.

However, this model does not represent the non-linear behavior of the tire. The linear tire model can be further extended to cover at least the maximal transferable force in each direction. The modified model is given as

$$F_x(\lambda) = \begin{cases} C_{\lambda 0}\lambda & \text{when} \quad C_{\lambda 0}\lambda \leq F_z\mu_{max} \\ F_z\mu_{max} & \text{when} \quad C_{\lambda 0}\lambda > F_z\mu_{max} \end{cases}, \tag{2.7}$$

$$F_y(\alpha) = \begin{cases} C_{\alpha 0}\alpha & \text{when} \quad C_{\alpha 0}\alpha \leq F_z\mu_{max} \\ F_z\mu_{max} & \text{when} \quad C_{\alpha 0}\alpha > F_z\mu_{max} \end{cases}, \tag{2.8}$$

where F_z is the normal load of the tire and μ_{max} is maximal friction coefficient.

This saturated tire model provides similar results in planar movement of the car as Pacejka's 'Magic' formula. These results are further discussed in section 2.2.3.

2.2.3 Tire models comparison

The longitudinal tire characteristics comparison is omitted since this thesis focuses mainly on the lateral dynamics of the vehicle. In figure 2.5 all lateral force characteristics of previously introduced tire models are shown.

For smaller side-slip angles $|\alpha| < 2$ all models mutually corresponds. The characteristics of the tire is linear in this range of side-slip angle. As the value of the side-slip angle increases, the Pacejka's 'Magic' formula reproduces the nonlinear behavior of the tire quite well.

The high precision tire models (Pacejka's 'Magic' formula and others) are often used for detailed simulation of the vehicle dynamics. However, the linear tire model with saturation is precise enough for needs of this thesis.

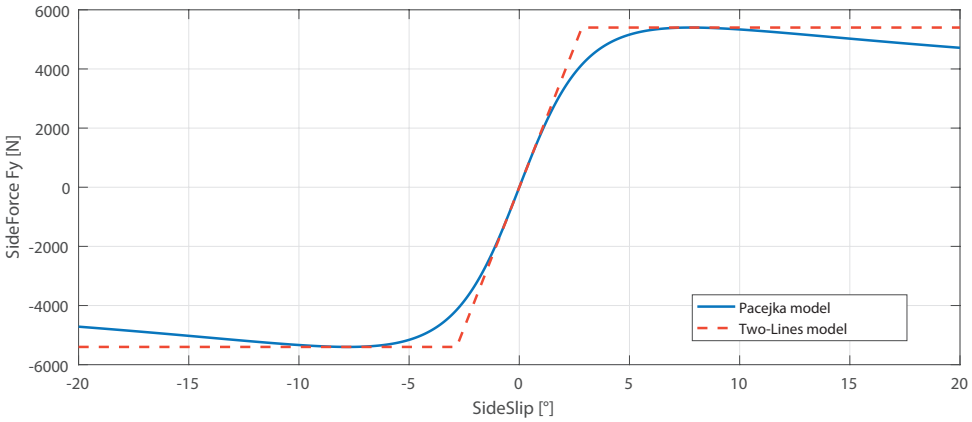

Normal force load $F_z = 6000$ N and friction $\mu = 0.9$.

Figure 2.5: Lateral force characteristics for different tire models

2.3 Kinematic vehicle model

The derivation of the kinematic vehicle model is based on a simple vehicle scheme, where the center of the corner is located on the line defined by the vehicle rear axle (see figure 2.6). The direction of movement of each point is in every case perpendicular to the line connecting the point and the center of the corner.

The intersection of normal to the direction of x-axis of the front tire and the rear axle of the vehicle gives the instantaneous cornering radius R. From figure 2.6 the vehicle states can be computed as

$$\dot{\psi} = \frac{v}{R} = \frac{v}{l_r} \tan(\beta), \tag{2.9}$$

$$\beta = \tan^{-1}\left(\frac{l_r}{l_r + l_f} \tan(\delta_f)\right), \tag{2.10}$$

where v is the vehicle speed, R is the cornering radius, δ_f is the front tire steer angle, l_f and l_r are distances of the centre of gravity of the car to the front and rear tire respectively, $\dot{\psi}$ is the vehicle yaw rate and finally β is the side-slip angle.

If the vehicle is going in a straight path, the radius of the curve approaches infinity, and the vehicle yaw rate and slip-angle are reaching 0. This vehicle model was initially developed in [14] and can be found in various titles such as [9].

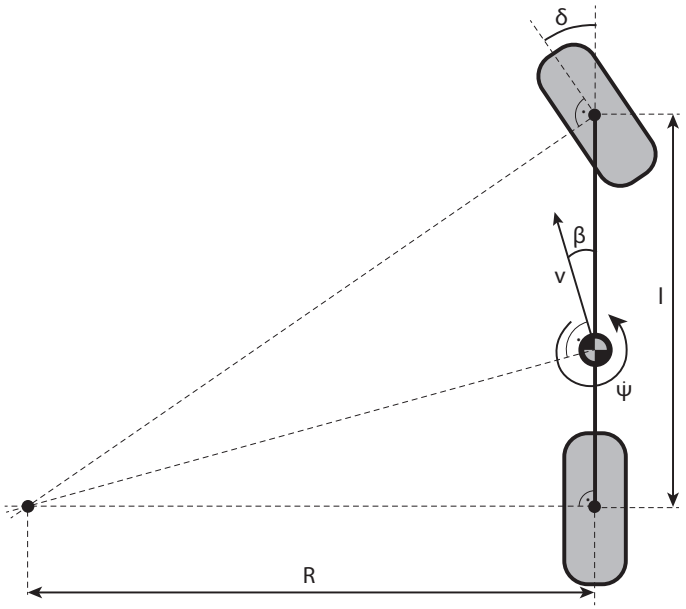

Figure 2.6: Mathematical vehicle model valid only for lower vehicle speeds.

2.4 Single track vehicle model

The complex vehicle models are usually used for accurate simulations of the vehicle movement. These models comprise nonlinear behavior of different vehicle parts (e.g., tire mechanics, drivetrain, brakes and road characteristics) and often describe all physical states of the moving vehicle and all of its parts. On the other hand, the kinematic vehicle model is sufficient for simplification of the design process of the vehicle control system. Only simple planar motion of the vehicle is considered and described in this thesis. Advanced vehicle models for various purposes can be found in [8, 18, 11, 5, 3, 16].

Typical road sports car is considered as the modeled vehicle. Therefore the vehicle center of gravity is projected into the plane of the surface to neglect the load transfer during the vehicle motion. Thus only one rotatory and two translatory degrees of freedom are required to estimate the current vehicle state sufficiently.

The vehicle coordinate system used within this thesis must be defined first (see fig. 2.7). The x axis of the vehicle points from the center of gravity towards the front of the vehicle and the y axis towards the left side of the vehicle from the driver's perspective. Finally, the z axis points up to follow commonly used the right-handed coordinate system.

The single-track vehicle model [14] describing planar vehicle motion is introduced in figure 2.8. The main difference between the real vehicle and

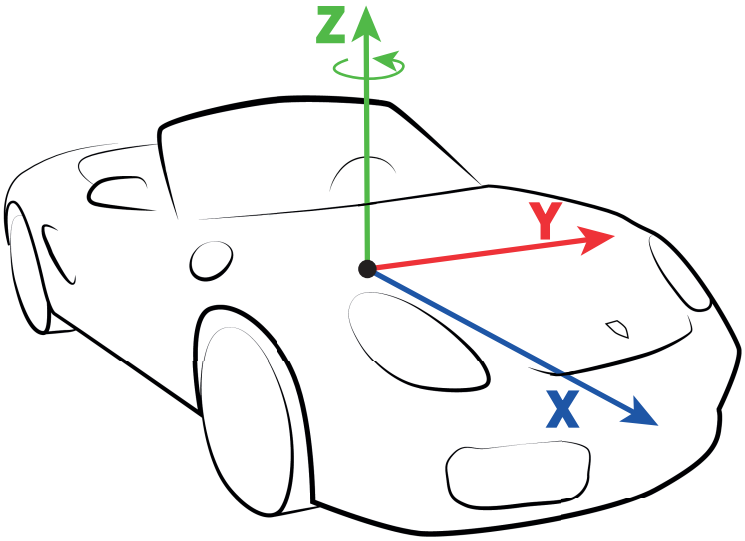

Figure 2.7: Vehicle coordinate system used within this thesis.

the presented scheme is the number of tires. The left and right front tires are replaced by one, which is placed into the center of front axis. The cornering stiffness coefficient has to be increased to include the influence of both original tires. The same principle is also used on the rear vehicle axle.

The vehicle in figure 2.8 is moving with velocity v. The angle between the x axis of the vehicle and the velocity vector is called the vehicle side-slip angle β and is defined as

$$\beta = \arctan\left(\frac{v_y}{v_x}\right), \tag{2.11}$$

where v_x and v_y are the vehicle velocities in x and y direction of the vehicle coordinate frame respectively.

An angle between the longitudinal vehicle axis x and fixed global axis x_0 is called vehicle yaw ψ. Vehicle acceleration $\dot{v}$ has the same direction as the vehicle velocity v if the vehicle motion is linear. If the vehicle is moving on curved track we observe centripetal acceleration a_c defined as

$$a_c = \frac{v^2}{R} = v(\dot{\beta} + \dot{\psi}), \tag{2.12}$$

where v is the instantaneous vehicle velocity, R instantaneous radius of the curved track, $\dot{\beta}$ is angular rate of the vehicle side-slip angle and $\dot{\psi}$ is the vehicle yaw rate about the vehicle z axis. However, the instantaneous radius of the motion is often unknown and changes frequently, thus only the second part of the equation with vehicle side-slip angle rate and yaw rate is normally used to compute the vehicle side acceleration.

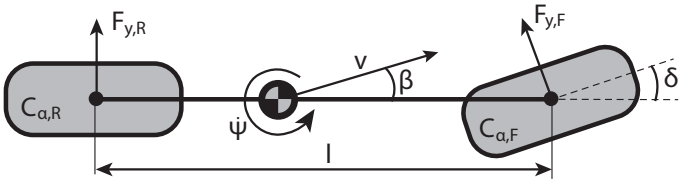

Figure 2.8: Single track model of the vehicle.

The differential equations of motion of the vehicle shown in figure 2.8 can be directly derived by creating equilibrium of all forces in the x (eq. 2.13) and y (eq. 2.14) vehicle direction and of all moments about the z axis (eq. 2.15) of the vehicle. The aerodynamic forces are neglected.

$$-m\dot{v}\cos(\beta)+mv(\dot{\beta}+\dot{\psi})\sin(\beta)-F_{y,F}\sin(\delta)+F_{x,F}\cos(\delta)+F_{x,R}=0 \quad (2.13)$$

$$-m\dot{v}\sin(\beta)-mv(\dot{\beta}+\dot{\psi})\cos(\beta)+F_{y,F}\cos(\delta)+F_{x,F}\sin(\delta)+F_{y,R}=0 \quad (2.14)$$

$$-I_z\ddot{\psi}+F_{y,F}l_f\cos(\delta)-F_{y,R}l_r+F_{x,F}l_f\sin(\delta)=0 \quad (2.15)$$

In differential equations of motion 2.13, 2.14 and 2.15, m is the mass of the vehicle, v is the velocity of the vehicle, $\dot{\psi}$ is the yaw rate of the vehicle,I_z is moment of inertia about the z axis, l_f and l_r are the distances of the centre of the front and rear tire from the vehicle gravity centre respectively, β is the slide-slip angle of the vehicle, δ is the front tire steering angle, $F_{x,F}$ and $F_{x,R}$ are longitudinal forces of front and rear tire respectively, $F_{y,F}$ and $F_{y,R}$ are lateral forces of front and rear tire respectively. The change of the side-slip angle $\dot{\beta}$ is very small compared to the yaw rate $\dot{\psi}$.

The tire forces $F_{y,F}$ and $F_{y,R}$ are defined within equations of selected tire model. The tire position and the steering angle has significant impact on side-slip angles of tires, which are defined as:

$$\alpha_F=\delta-\arctan\left(\frac{v\sin(\beta)+l_f\dot{\psi}}{v\cos(\beta)}\right), \quad (2.16)$$

$$\alpha_R=-\arctan\left(\frac{v\sin(\beta)-l_r\dot{\psi}}{v\cos(\beta)}\right), \quad (2.17)$$

where α_F and α_R are tire side-slip angles of the front and the rear tire respectively.

The relations 2.16 and 2.17 can be approximated for small steering angles as:

$$\alpha_F=\delta-\beta-\frac{l_f\dot{\psi}}{v_x}, \quad (2.18)$$

$$\alpha_R = -\beta + \frac{l_r \dot{\psi}}{v_x}. \tag{2.19}$$

The equations 2.13 - 2.17 describe the single track vehicle model for planar motion. The vehicle model derived above is in following chapters linearized and used to develop torque vectoring control algorithms.

2.5 Linear vehicle model with constant velocity

Assuming front wheel steering angle δ and side-slip angle β smaller than 10°, the single track vehicle model from section 2.4 can be linearized using equations

$$\sin(x) \approx x, \qquad \cos(x) \approx 1. \tag{2.20}$$

The vehicle differential equations of motion 2.13, 2.14 and 2.15 can be reformulated using equation 2.20 to

$$-m\dot{v} + F_{x,F} + F_{x,R} = 0, \tag{2.21}$$

$$-mv(\dot{\beta} + \dot{\psi}) + F_{y,F} + F_{y,R} = 0 \quad \text{and} \tag{2.22}$$

$$-I_z\ddot{\psi} + F_{y,F}l_f - F_{y,R}l_r = 0. \tag{2.23}$$

The side-slip angles of the front and rear tire are defined in equations (2.18) and (2.19) respectively. The lateral tire forces $F_{y,F}$ and $F_{y,R}$ can be estimated using linear model described in section 2.2.2.

The acceleration of the vehicle $\dot{v}$ is assumed to be equal to zero during the cornering maneuver with constant velocity. The vehicle differential equations are after substitution of side forces $F_{y,F}$ and $F_{y,R}$ (see eq. 2.6) and using equations 2.18 and 2.19 transformed into following equations

$$-mv\dot{\beta} - mv\dot{\psi} + C_{\alpha 0,F}\left(\delta - \beta - \frac{l_f\dot{\psi}}{v}\right) + C_{\alpha 0,R}\left(-\beta + \frac{l_r\dot{\psi}}{v}\right) = 0, \tag{2.24}$$

$$-I_z\ddot{\psi} + C_{\alpha 0,F}\left(\delta - \beta - \frac{l_f\dot{\psi}}{v}\right)l_f - C_{\alpha 0,R}\left(-\beta + \frac{l_r\dot{\psi}}{v}\right)l_r = 0. \tag{2.25}$$

The linearized differential equations can be modified after small manipulation into following state space model:

$$\begin{bmatrix}\dot{\beta}\\ \ddot{\psi}\end{bmatrix} = \begin{bmatrix} -\frac{C_{\alpha 0,F}+C_{\alpha 0,R}}{mv} & -\left(1 + \frac{C_{\alpha 0,F}l_f - C_{\alpha 0,R}l_r}{mv^2}\right) \\ -\frac{C_{\alpha 0,F}l_f - C_{\alpha 0,R}l_r}{I_z} & -\frac{C_{\alpha 0,F}l_f^2 + C_{\alpha 0,R}l_r^2}{I_z} \end{bmatrix} \begin{bmatrix}\beta\\ \dot{\psi}\end{bmatrix} + \begin{bmatrix}\frac{C_{\alpha 0,F}}{mv}\\ \frac{C_{\alpha 0,F}l_f}{I_z}\end{bmatrix}\delta, \tag{2.26}$$

where the vehicle states are represented by the vehicle side-slip angle β and the vehicle yaw rate $\dot{\psi}$.

The linear vehicle model with constant velocity is analyzed in chapter 3. Parameters of the vehicle are fitted and validated in chapter 4 to match the values from real test vehicle.

2.5.1 Linear model and with yaw moment as input

The linear vehicle model with constant velocity and all mathematical models described above does not have any physical input, which can simulate the torque vectoring system.

The torque vectoring system is represented as a difference between the torques on the right and left electric motor of the vehicle. This difference of torques creates the torque vectoring yaw moment M_z about the z-axis of the vehicle.

This additional yaw moment can be computed as follows

$$M_z = \left(\frac{TQ_R - TQ_L}{r}\right)\frac{w}{2}, \tag{2.27}$$

where w is the rear track of the vehicle, r is the diameter of the rear tires and TQ_R and TQ_L are torques on the right and left wheel respectively.

The additional yaw moment can be directly placed into the third equation of motion - the sum of the moments. After simple manipulation similar to the derivation of the linear vehicle model with constant speed linear vehicle model (eq. 2.28) with torque vectoring input is obtained.

$$\begin{bmatrix}\dot{\beta}\\ \ddot{\psi}\end{bmatrix} = \begin{bmatrix} -\frac{C_{\alpha 0,F}+C_{\alpha 0,R}}{mv} & -\left(1+\frac{C_{\alpha 0,F}l_f - C_{\alpha 0,R}l_r}{mv^2}\right)\\ -\frac{C_{\alpha 0,F}l_f - C_{\alpha 0,R}l_r}{I_z} & -\frac{C_{\alpha 0,F}l_f^2 + C_{\alpha 0,R}l_r^2}{I_z}\end{bmatrix}\begin{bmatrix}\beta\\ \dot{\psi}\end{bmatrix} + \begin{bmatrix}\frac{C_{\alpha 0,F}}{mv} & 0\\ \frac{C_{\alpha 0,F}l_f}{I_z} & \frac{1}{I_z}\end{bmatrix}\begin{bmatrix}\delta\\ M_z\end{bmatrix} \tag{2.28}$$

Chapter 3

Linear analysis

3.1 Introduction

In the previous chapter, the linear constant velocity vehicle model was derived and described. This simple model can be later used for designing of the control systems.

The linear constant velocity vehicle model (eq. 2.26) is a simple second order linear state-space model with only one input (the steering angle of the front wheel δ), two internal states (vehicle side-slip angle β and yaw rate $\dot{\psi}$) and several parameters to modify its behavior. However, each of the physical parameters influences the static and dynamic characteristics of this model in its own way.

Therefore, it is essential for the control engineers to understand, what are the impacts of variations in mass and geometric parameters of the vehicle to the time constants, natural frequencies and damping ratios of the lateral model modes. The description of these dependencies is the goal of this chapter. The knowledge of this area can later help with parameterization of the vehicles models to match the real parameters and also with evaluation of the results of vehicle control systems experiments.

Some results presented in this chapter were published in a conference paper [12]. The parameterization of the vehicle model in this chapter was selected to match a typical passenger car. Only one selected parameter is varied in each subsection. The influence on the location of roots of a characteristic polynomial is shown and described in each subsection. The time response of the vehicle yaw rate to the step change of the direction of the front wheels together with the Bode plot is presented. Each figure contains arrows which indicate the direction of change as the value of selected parameter increase.

Weight m	1500 kg
Vehicle speed v	15.5 m s^{-1}
Moment of inertia I_z	2000 kg m^2
Vehicle length	3 m
Distance of front wheel and CG l_f	1.3 m
Distance of rear wheel and CG l_r	1.7 m
Nominal cornering stiffness of front tire $C_{\alpha 0,F}$	100000 N rad^{-1}
Nominal cornering stiffness of rear tire $C_{\alpha 0,R}$	120000 N rad^{-1}

Table 3.1: Default parameter values of the vehicle model.

3.2 Vehicle velocity

The parameter, which has one of the biggest influence on vehicle handling during the vehicle cornering, is the velocity of the moving vehicle. The velocity v appears only in denominators of components of the system matrix A (eq. 2.26). Therefore, as the velocity increases, the poles of the system should move towards zero in the left half of the pole-zero plot.

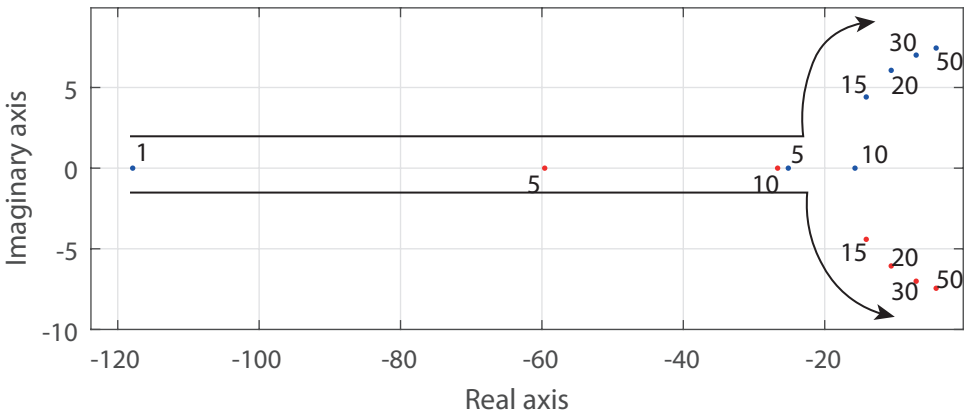

Figure 3.1: Change of the pole location of the linear constant velocity vehicle model by the velocity increment.

The tendency mentioned above is shown in figure 3.1. As the vehicle velocity v increases, the poles of the system moves towards zero (indicated by black arrow). At some point, the real poles gain nonzero imaginary part, which is further increased.

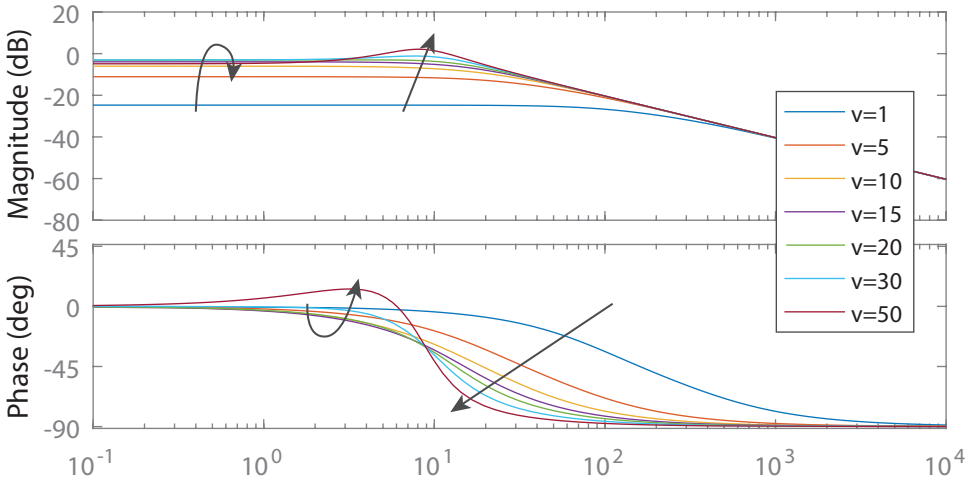

Figure 3.2: Change of the Bode plot of linear constant velocity vehicle model by the velocity increment.

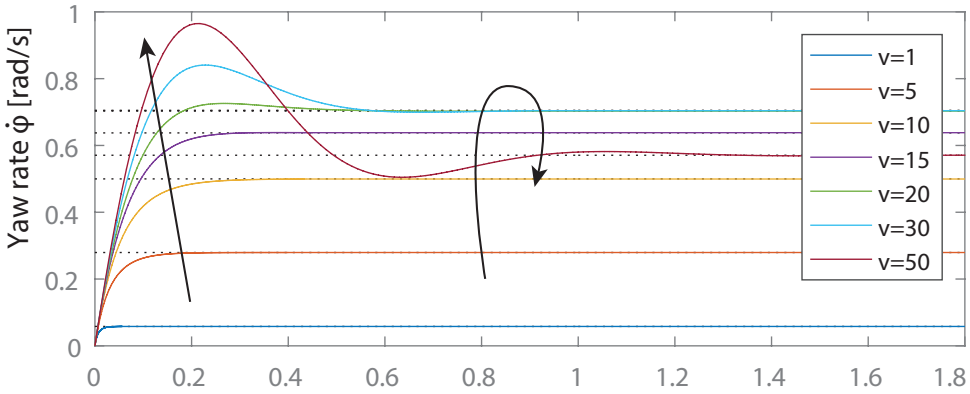

Figure 3.3: Change of the step response of linear constant velocity vehicle model to the change of the front tires direction by the velocity increment.

The nonzero imaginary part of the poles of the system has another effect on vehicle handling. This effect can be seen in the time response of the linear system to the step change of the direction of the front wheels (fig. 3.3, 3.4). As the vehicle velocity increases, the vehicle yaw rate $\dot{\phi}$ (steady state) also increases up to the critical value. With further increase of the vehicle velocity, the (steady-state value of) yaw rate decreases which results in larger radius of the corner. The vehicle can also became unstable in the terms of the poles location if the vehicle speed exceeds the critical limit. More information about the critical vehicle speed is in section 3.6.1.

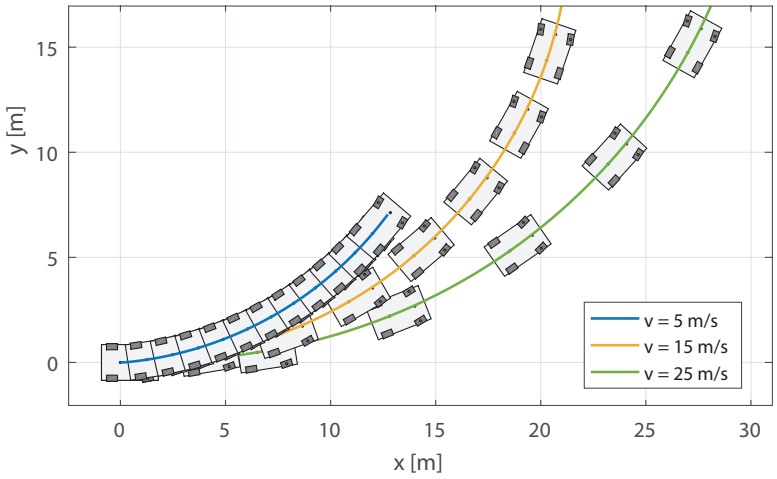

Figure 3.4: Change of the planar movement of the linear constant velocity vehicle model as the velocity increases. The vehicles are displayed every 0.3 s.

3.3 Position of the centre of gravity

Another interesting parameter influencing the vehicle handling is the location of the center of gravity. The change of the location of the centre of gravity is represented in figures 3.5, 3.6 and 3.7 as the increasing distance l_f between the front wheel and the centre of gravity. The length of the vehicle remains the same, thus the distance between the rear wheel and the center of gravity l_r decreases. The vehicle velocity was set constant to $v = 15.5\ \mathrm{m\,s^{-1}}$.

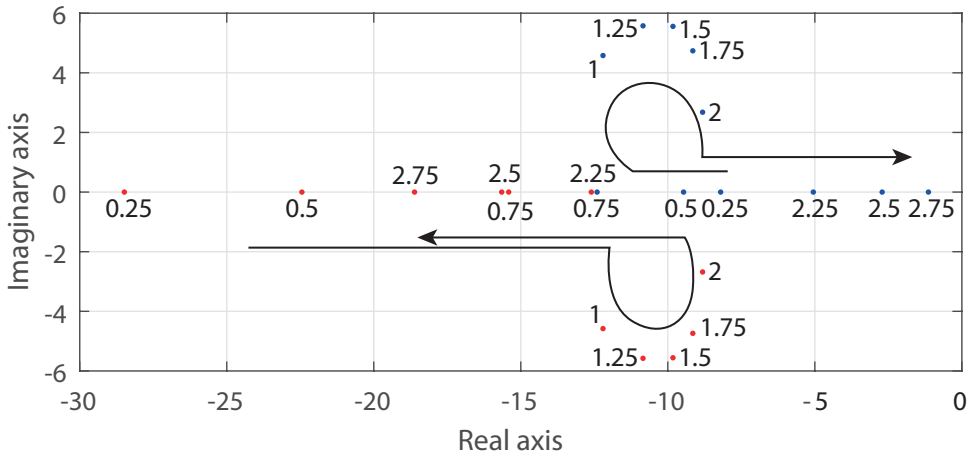

Figure 3.5: Change of the pole locations of linear vehicle model as the distance of CG and front wheel increases. The distance of the CG and rear axle decreases with the same rate.

The common knowledge says that movement of the center of gravity

towards the front wheel creates quicker vehicle response and less rear wheel grip. Moving the center of gravity towards the rear axle does the opposite - less steering and more rear wheel grip. However, the influence of the location of the center of gravity on the normal loads of the tires is neglected in this simulation, and only the impacts of the lateral tire forces are studied.

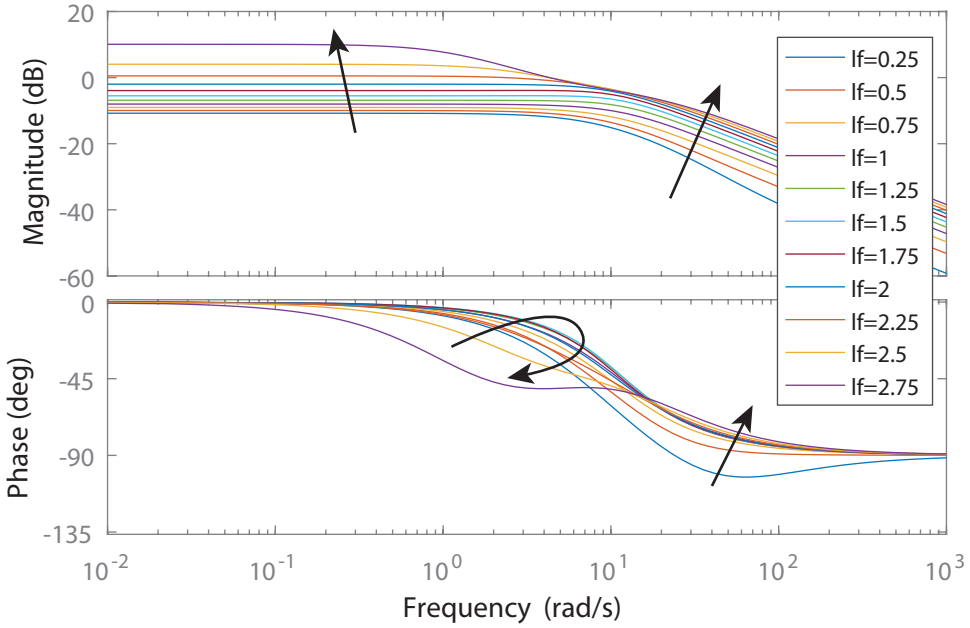

Figure 3.6: Change of the Bode plot of linear vehicle model as the distance of CG and front wheel increases. The distance of the CG and rear axle decreases with the same rate.

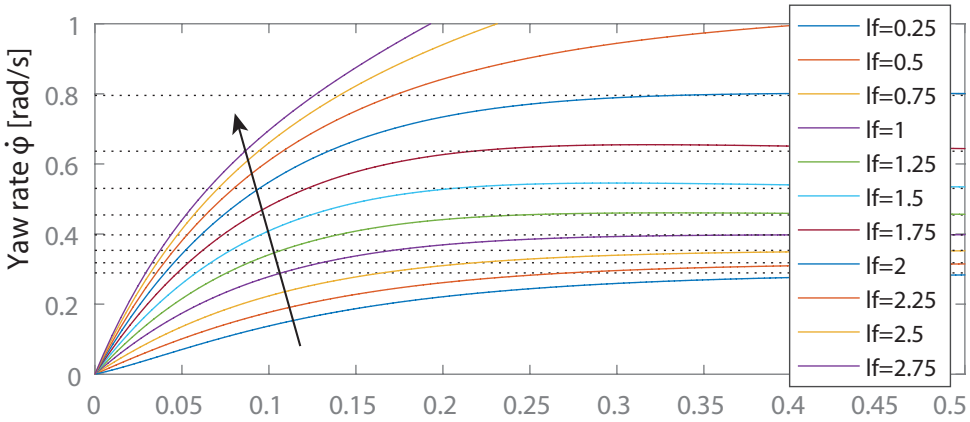

Figure 3.7: Change of the step response of linear vehicle model to the change of the front tires direction as the distance of CG and front wheel increases. The distance of the CG and rear axle decreases with the same rate.

The response of the linear vehicle system to the step change of the direction of the front wheels shown in figure 3.7. The change of the vehicle behavior

is easily seen. The rising time of the response decreases up to the moment, where the center of gravity is closer to the front wheel ($l_f = 1.25$ m). Then the rising time grows again. The gain of the response is rising as the distance between the CG and the front wheel is increased.

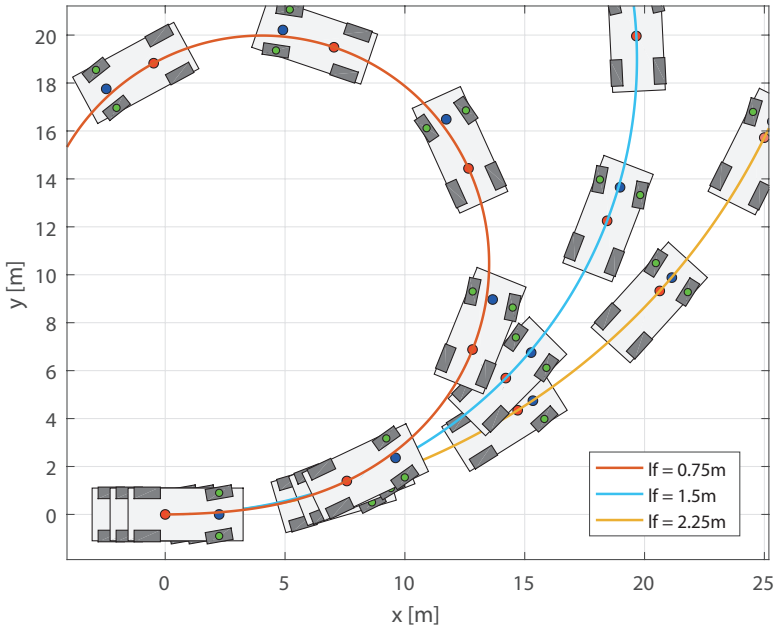

Figure 3.8: Change of the planar movement of linear vehicle model as the distance of CG and front wheel increases. The distance of the CG and rear axle decreases with the same rate. The vehicle is displayed every 0.5 s.

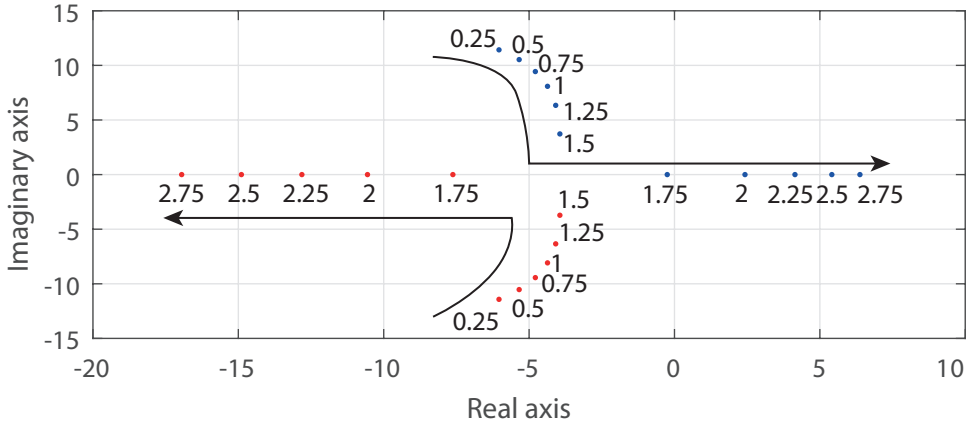

Figure 3.9: Change of the poles location of linear vehicle model at higher velocity as the distance of CG and front wheel increases. The distance of the CG and rear axle decreases with the same rate.

The planar position of the vehicle during the system response to the front wheel turn is shown in figure 3.8. This figure shows that the position of

the center of gravity of the vehicle has a significant influence on the turning moment generated by the front and rear tires.

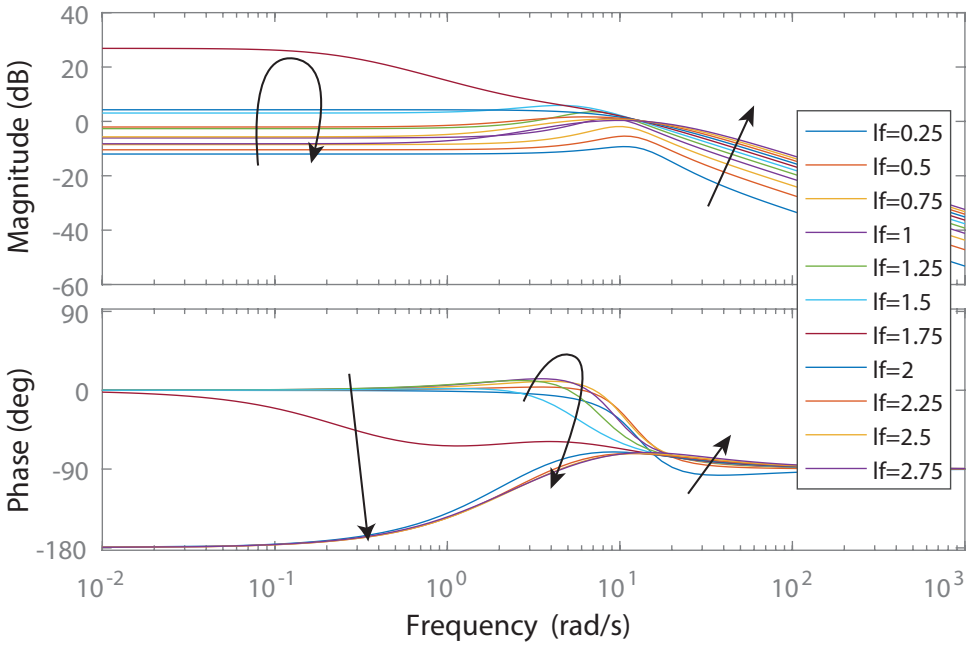

Figure 3.10: The change of the Bode plot of linear vehicle model at higher velocity as the distance of CG and front wheel increases. The distance of the CG and rear axle decreases with the same rate.

The change of the location of the poles is different when the vehicle is moving with higher velocity. The vehicle velocity was set to $v = 50$ m/s for following simulations. If the center of gravity is close to the rear wheel, the vehicle can become unstable regarding the location of the poles. This behavior is shown in figures 3.9, 3.10 and 3.11. If the distance of the vehicle center of gravity and the front axle is higher than 1.75 m, one of the poles has positive real value. More information about the poles are presented in section 3.6.1.

The planar movement of the vehicle during the dynamic response of the model to the step change in the direction of the front tires is shown in figure 3.12. The cornering radius of the vehicle is decreasing as the distance between the front axle and the center of gravity of the vehicle increases. The planar position also shows the non-stable time response of the linear system from figure 3.11 for $l_f = 2.25$ m.

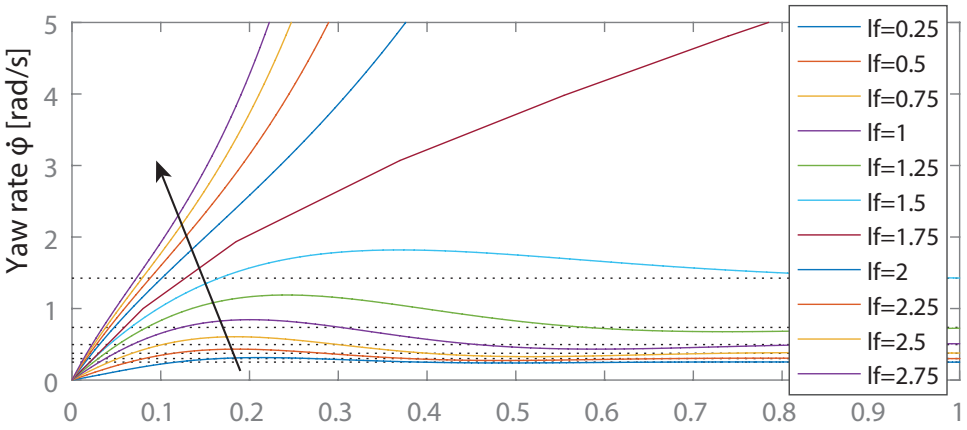

Figure 3.11: The change of the step response of linear vehicle model to the change of the front tires direction at higher velocity as the distance of CG and front wheel increases. The distance of the CG and rear axle decreases with the same rate.

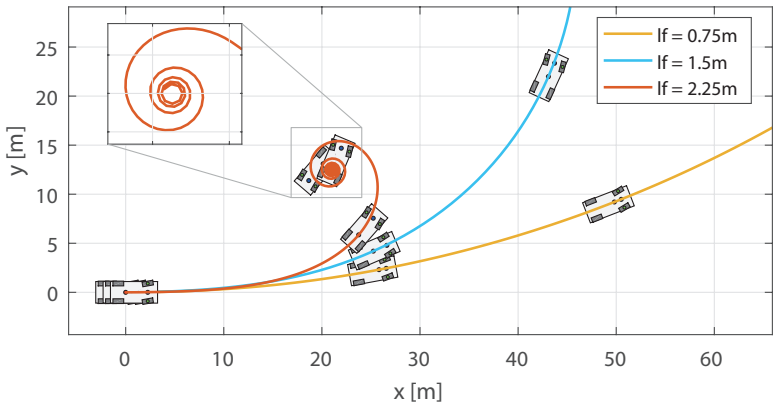

Figure 3.12: Change of the planar movement of linear vehicle model at higher velocity as the distance of CG and front wheel increases. The distance of the CG and rear axle decreases with the same rate. The vehicle velocity was set to $v = 50\ \mathrm{m\,s^{-1}}$. The vehicle is displayed every 0.5 s.

3.4 Moment of inertia

The moment of inertia is varied in this subsection. This parameter can be physically changed by moving the vehicle engine and transmission from the centre of the vehicle to the front and back of the vehicle or using a different material for the vehicle body. The vehicle center of gravity should remain in the same location.

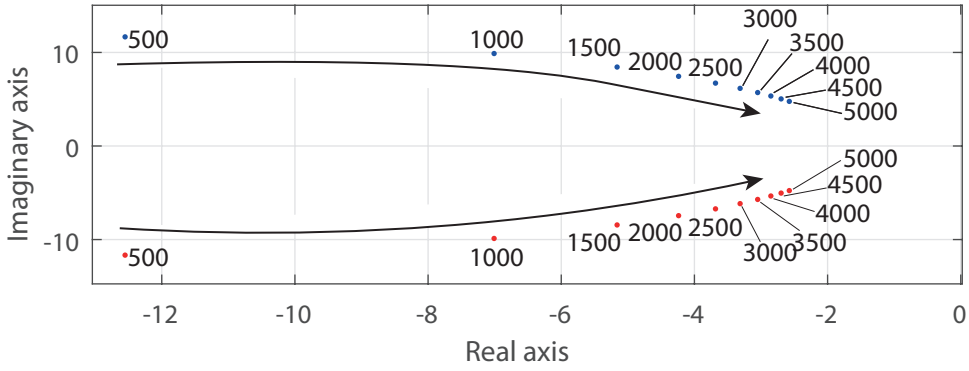

Figure 3.13: Change of the poles location of linear vehicle model as the vehicle moment of inertia increases. The vehicle weight remains unchanged.

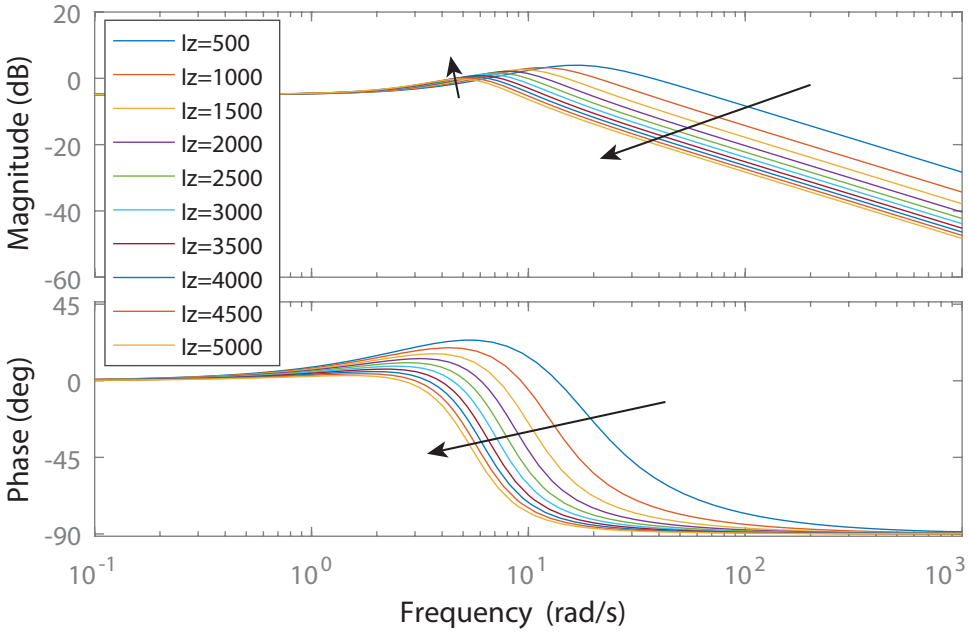

Figure 3.14: Change of the Bode plot of linear vehicle model as the vehicle moment of inertia increases. The vehicle weight remains unchanged.

The common practice of the sports vehicle design is to keep the moment of inertia of the entire vehicle as small as possible. The time response of the system (fig. 3.13) together with the planar position of the vehicle (fig. 3.16) confirms this practice. As the moment of inertia increases, the time response of the system output is slower, and the vehicle gains more understeer behavior.

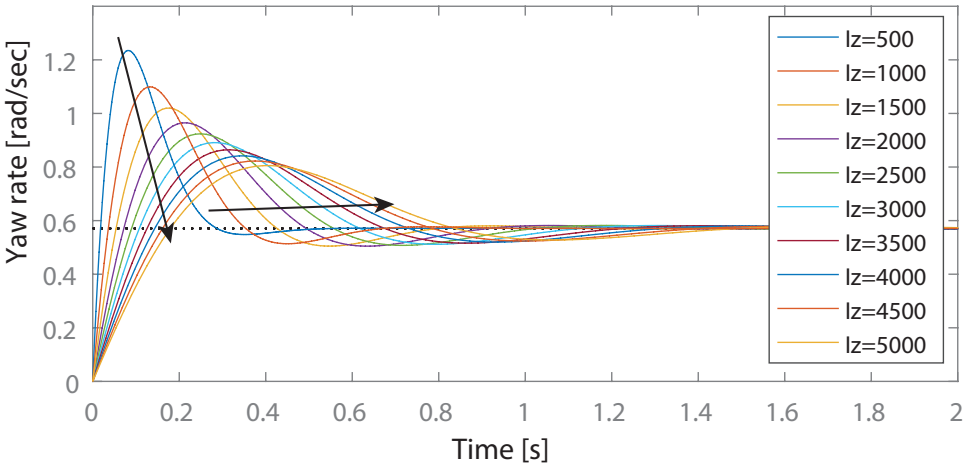

Figure 3.15: Change of the step response of linear vehicle model to the change of the front tires direction as the vehicle moment of inertia increases. The vehicle weight remains unchanged.

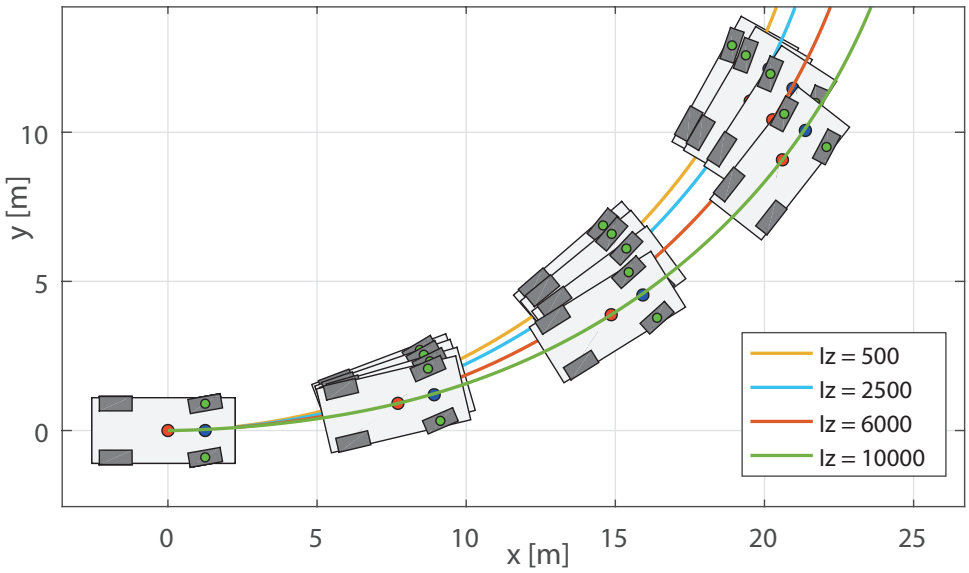

Figure 3.16: Change of the planar movement of linear vehicle model as the vehicle moment of inertia increases. The vehicle weight remains unchanged. The vehicle is displayed every 0.5 s.

3.5 Vehicle weight

Additional weight in the vehicle usually changes the moment of inertia of the vehicle. However, it is assumed in this subsection, that the weight is added only to the vehicle center of gravity. Thus the moment of inertia is not modified. This modification can be achieved for example by adding or

removing some weight of the motor of the mid-engine vehicle since the motor is usually placed near the center of gravity of this vehicle.

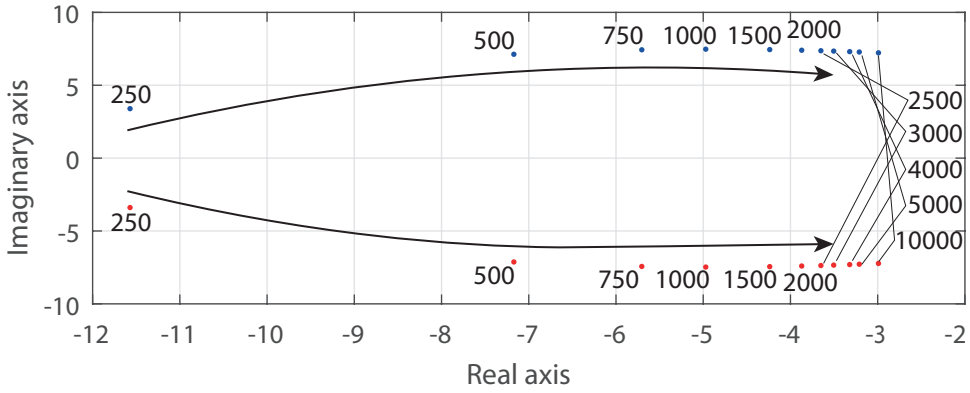

Figure 3.17: Change of poles location of linear vehicle model as the vehicle weight increases. The vehicle moment of inertia remains unchanged.

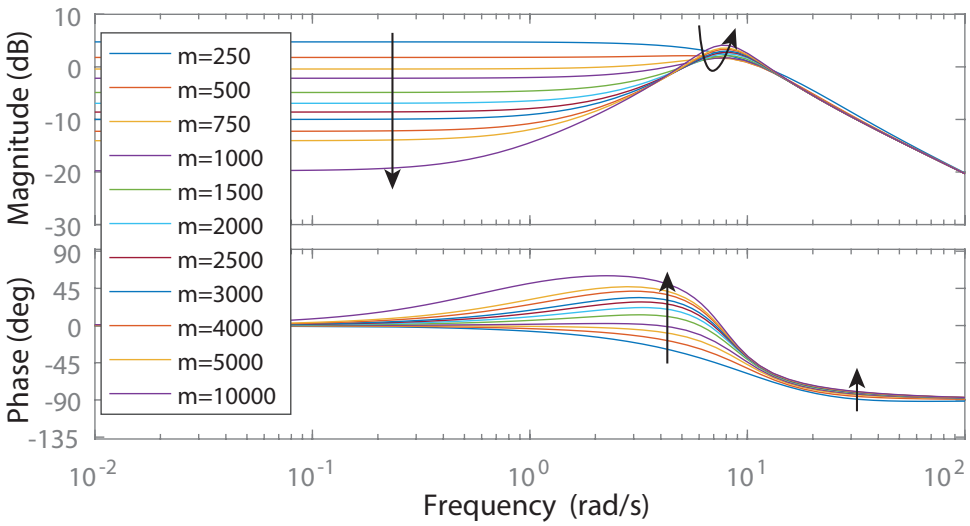

Figure 3.18: Change of the Bode plot of linear vehicle model as the vehicle weight increases. The vehicle moment of inertia remains unchanged.

Additional vehicle weight added to the vehicle center of gravity results in the smaller yaw rate and less dumped yaw rate response of the vehicle. These phenomena correspond with common sense - as the vehicle gains weight the vehicle tends to understeer. If we remove some weight, we can achieve higher yaw rate and quicker vehicle response for the same steering angle. Comparison of selected responses is shown in the figure 3.20.

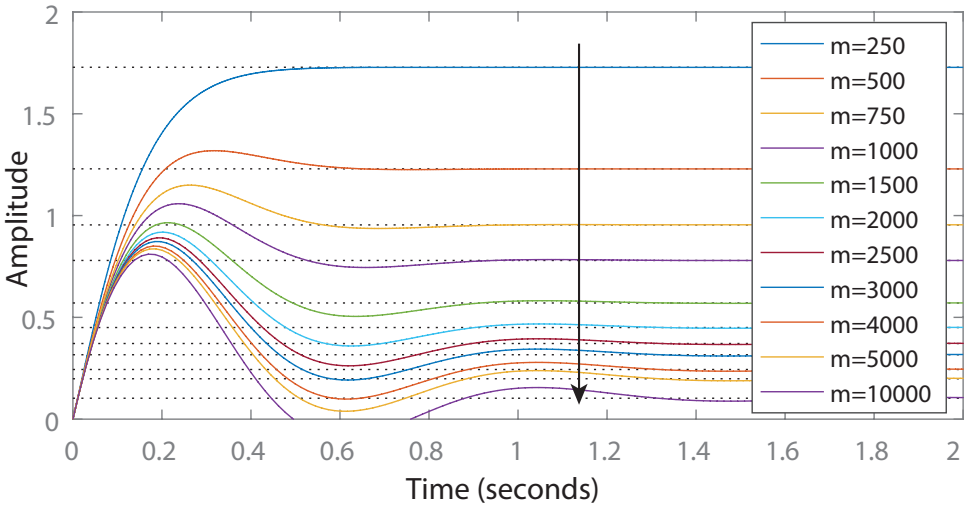

Figure 3.19: Change of the response of linear vehicle model to the change of the front tires direction as the vehicle weight increases. The vehicle moment of inertia remains unchanged.

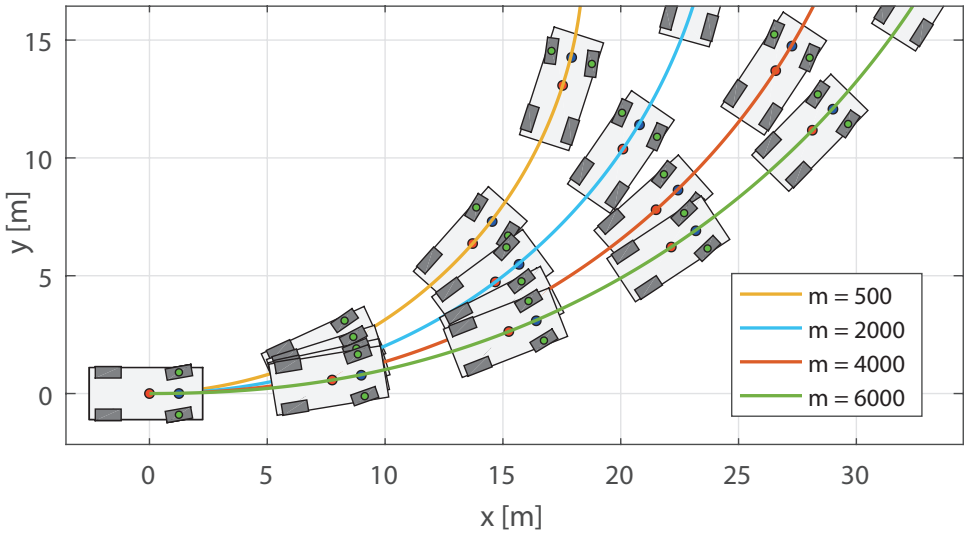

Figure 3.20: Planar position of the linear vehicle model as the vehicle velocity increases. The vehicle is displayed every 0.5 s.

3.6 Additional properties of linear vehicle model

3.6.1 Critical speed

The stability of the linear steady-state cornering model developed in section 2.5 can be determined by examining the two eigenvalues λ_1 and λ_2 of this system.

The eigenvalues of the linear constant velocity vehicle model are solutions of the characteristic equation

$$\det(\mathbf{A} - \lambda \mathbf{I}) = 0. \tag{3.1}$$

The system is asymptotically stable if and only if both eigenvalues have negative real parts.

$$\text{system is stable} \iff \text{Re}(\lambda_1) < 0 \text{ and } \text{Re}(\lambda_2) < 0 \tag{3.2}$$

If one of the eigenvalue has positive real part, the system is not stable and grows in time without bounds. The eigenvalues of the linear constant velocity vehicle model can be expressed as

$$\lambda_{1,2} = -\text{tr}(\mathbf{A}) \pm \sqrt{\text{tr}(\mathbf{A})^2 - \det(\mathbf{A})^2} \tag{3.3}$$

where trace and determinant of the system matrix $\mathbf{A}$ are obtained analytically as

$$\text{tr}(\mathbf{A}) = \frac{1}{v}\left(\frac{C_{\alpha,F} l_f^2 + C_{\alpha,R} l_r^2}{I_z} + \frac{C_{\alpha,F} + C_{\alpha,R}}{m}\right) \geq 0, \tag{3.4}$$

$$\det(\mathbf{A}) = -\frac{C_{\alpha,F} l_f - C_{\alpha,R} l_r}{I_z} - \frac{1}{v^2}\frac{(C_{\alpha,F} l_f - C_{\alpha,R} l_r)^2}{m I_z} - \\ - \frac{1}{v^2}\frac{\left(C_{\alpha,F} l_f^2 - C_{\alpha,R} l_r^2\right)}{m I_z}. \tag{3.5}$$

The critical vehicle velocity is obtained by solving the equation 3.3 for numbers with real part less than 0:

$$v_{crit} = \sqrt{\frac{C_{\alpha,F} C_{\alpha,R} (l_f + l_r)^2}{m\,(I_z + C_{\alpha,F} l_f - C_{\alpha,R} l_r)}}, \tag{3.6}$$

where v_{crit} is so-called critical speed. The vehicle becomes unstable if its speed reaches or exceeds this value. This equation also shows, that the vehicle dynamics, stability and behavior highly depends on the velocity.

The critical vehicle velocity v_{crit} can be computed only for linear constant vehicle model with parameterizations with oversteering behavior. The parameters then satisfy the following condition to compute critical vehicle velocity

. (3.7)

The dependency of the critical vehicle velocity on the vehicle weight is shown in the figure 3.21. As the vehicle weight grows, the velocity during the point at which the vehicle becomes unstable regarding the location of the system poles is decreasing. The same behavior can be seen in figure 3.23, but the influence of the vehicle moment of inertia is not as significant as the weight influence.

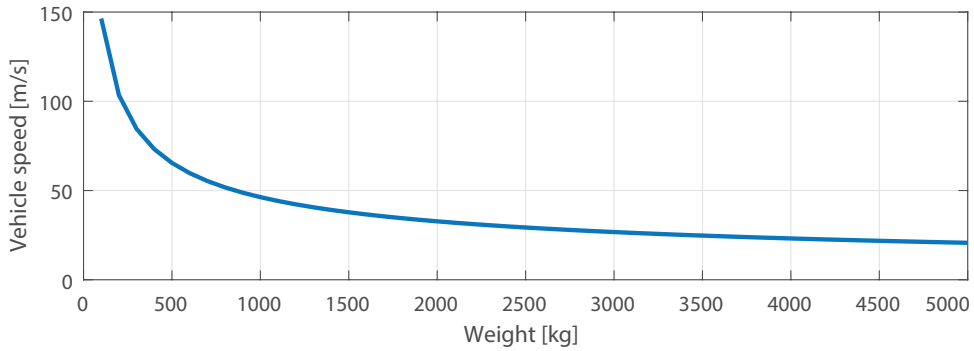

Figure 3.21: The dependency of the critical vehicle velocity on the vehicle weight.

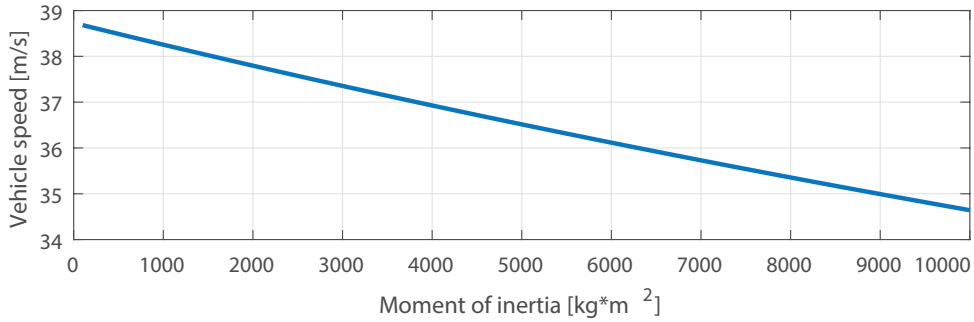

Figure 3.22: The dependency of the critical vehicle velocity on the vehicle moment of inertia.

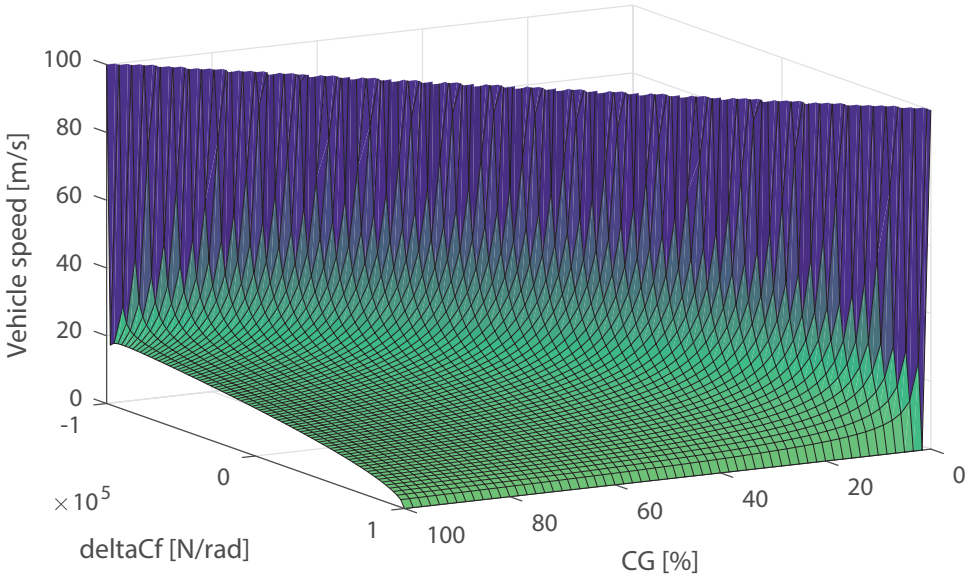

Figure 3.23: The dependency of the critical vehicle velocity on the position of the centre of gravity of the vehicle and the difference between the front and rear tire cornering stiffness.

Chapter 4

Parameterization and vehicle simulation

4.1 Introduction

The implementation of developed control systems and evaluation of results on actual test vehicle is the primary goal of this thesis. The single track vehicle model used for simulations and linearized constant velocity vehicle model used for control design must match the real dynamic behavior of the test vehicle not only to obtain good simulation results but also to support better design of the control system.

In this chapter, the electric test vehicle used for the torque vectoring experiments is briefly presented. Then all measurable parameters of the test vehicle are given. Next, the values of remaining parameters are defined experimentally using simulation results of vehicle step steer tests. Finally, all presented parameters are validated by simple experiments with the vehicle dynamics and handling.

4.2 Test Vehicle

The test vehicle used for validation of control algorithms developed within this thesis is similar to Porsche Boxster S. The original combustion engine was replaced with two electric motors for each rear wheel and battery pack was added to power the whole vehicle.

All parameters in following sections were measured or precisely tuned to closely match the results of the kinematic vehicle model and the linearized constant speed vehicle model and the real behavior of this test vehicle.

Figure 4.1: The test vehicle for torque vectoring. Flashing new version of the electric vehicle control system into the test vehicle on a closed airfield.

4.3 Vehicle parameters

4.3.1 Measurable vehicle parameters

Test vehicle parameters such as a distance between front and rear tires are taken from the technical documents [1]. Other parameters such as total weight or the weight distribution or steering wheel ratio were computed or measured manually. The list of measured vehicle parameters is presented in table 4.1.

Wheelbase l	2415 mm
Front track f	1486 mm
Rear track w	1528 mm
Distance of front wheel and CG l_f	1433 mm
Distance of rear wheel and CG l_r	982 mm
Total vehicle weight m	1700 kg

Table 4.1: The test vehicle parameters

The total weight of the vehicle is a sum of the weight of the test vehicle (1540 kg) and the weight of two passengers (80 kg each).

The only possible way to measure actual front wheel direction in the vehicle is to compute it from the vehicle steering angle. Therefore, the ratio between the steering angle and the front wheel angle is significant for the precision

of the vehicle models. Unfortunately, this conversion is usually non-linear because of the vehicle front axle design.

An example of the nonlinear characteristics of the steering wheel angle and the front wheel angle conversion is in figure 4.2.

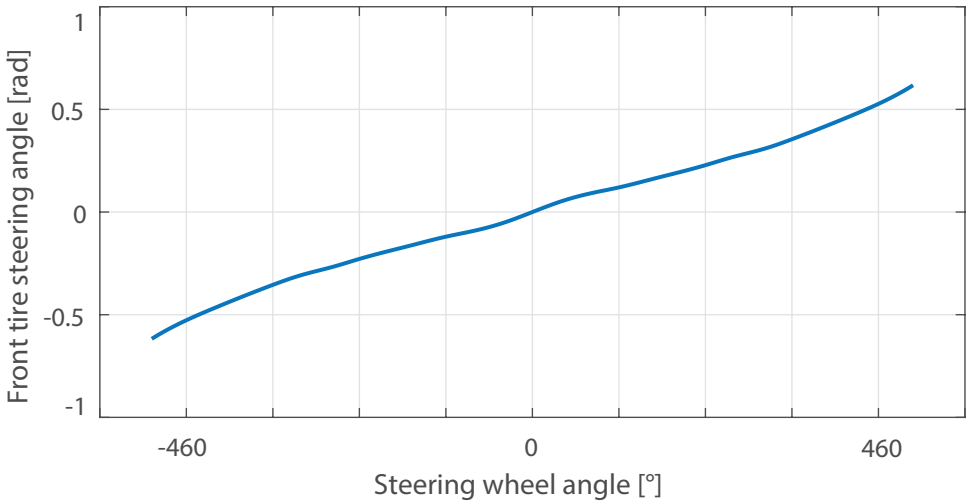

Figure 4.2: Example of the nonlinear characteristics between steering wheel angle and the front tire steering angle.

4.3.2 Experimentally identified vehicle parameters

With knowledge from the chapter 3, the rest of the vehicle parameters was experimentally modified concerning the vehicle dynamics response to the step steering. The results of simulations were compared to the step steer tests performed with the test vehicle.

Front stiffness coefficient $C_{\alpha 0,F}$	85000 $\mathrm{N\,rad^{-1}}$
Rear stiffness coefficient $C_{\alpha 0,R}$	110000 $\mathrm{N\,rad^{-1}}$
Moment of inertia I_z	3500 $\mathrm{kg\,m^{-2}}$

Table 4.2: Empirical vehicle parameters

The front and rear stiffness coefficients are valid for the single track vehicle model. Therefore it contains dynamic behavior of both front and both rear tires respectively.

In figure 4.3 an example of different values of front stiffness coefficients is compared. Vehicle yaw rate represents the vehicle response. The simulation input is a real step input from the driver (with limited slope). The step steer

test was performed at 50 km h^{-1}. The yaw rate vehicle response with the selected value of the stiffness coefficient of the front tire (85000 N rad^{-1}, tab. 4.2) matches the real yaw response of the test vehicle quite well.

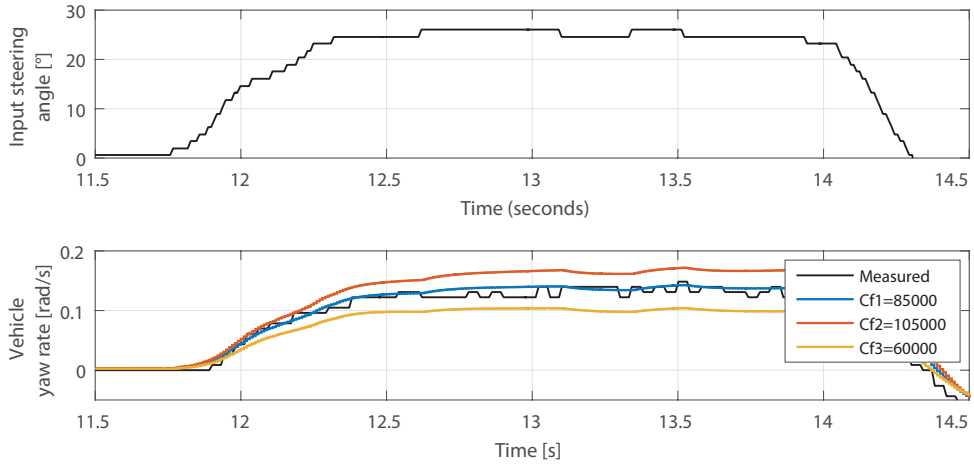

Figure 4.3: Front stiffness coefficient fitting. An example of fitting the front stiffness coefficient. Simulated yaw rate should match the values from the vehicle step steer test.

4.4 Parameter validation

The vehicle models developed in chapter 2 were parameterized with the vehicle data listed in the previous sections. The data from two different vehicle dynamics tests were recorded using professional CAN network interface by Vector[1]. The data were then compared with the simulation results of the models. The measured data of the front tire steering angle (calculated from the steering wheel angle) as well as the velocity of the vehicle were used as inputs for all simulated models.

4.4.1 Slow speed steer

This vehicle experiment was performed in a closed parking lot. The vehicle velocity did not exceed 15 km h^{-1}, and the input from the steering wheel was smooth without significant and sudden changes. In this case, the test vehicle should have the same behavior as the kinematic model and together with the single track vehicle model and its linearized version.

The measured and simulated yaw rate in figure 4.4 is nearly the same for kinematic vehicle model and linear constant velocity vehicle model. The linear

[1] Vector Informatik GmbH. `www.vector.com`

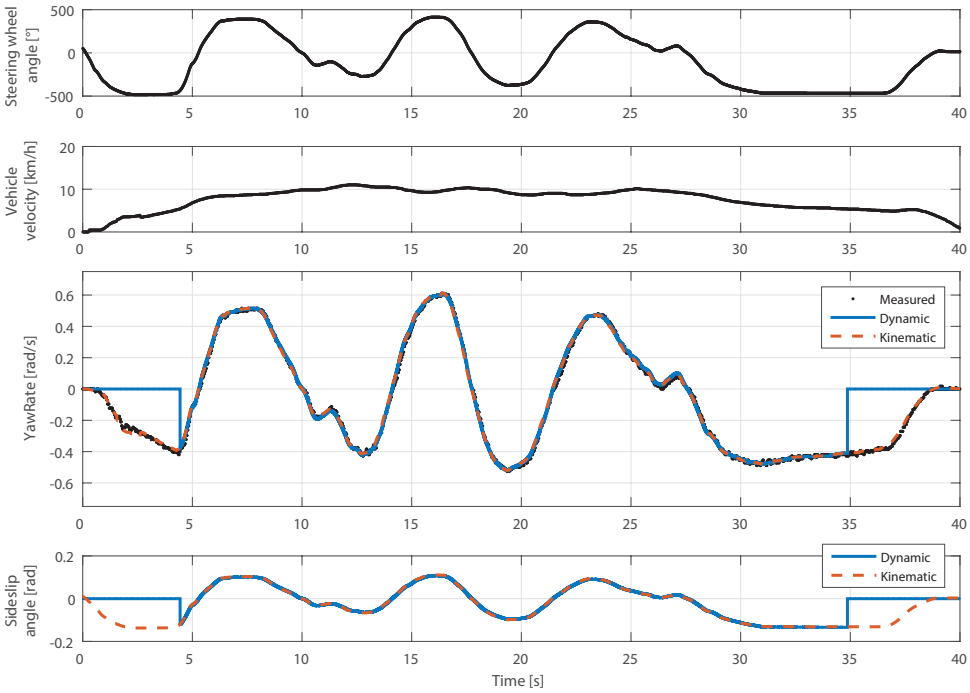

Figure 4.4: Slow speed steering. Comparison of real measured values with simulated values. The data labeled 'Dynamic' represents the linear constant velocity vehicle model.

constant velocity vehicle model generates meaningless data if the vehicle speed is around 0. Therefore the condition for the enabling of the computation was set to $v \geq 1.5\mathrm{m\,s^{-1}}$. In the real application of control systems containing the reference values (5.3.1), the switching between the kinematic and linear constant velocity vehicle models will be necessary. More detailed description of the implementation for the target is in sections 5.3.1 and 5.4.

4.4.2 High-speed steer

Similar vehicle experiment was performed on a closed airfield. The data presented in figure 4.5 were measured at the vehicle speeds around 100 $\mathrm{km\,h^{-1}}$. The steering wheel input was smooth, without fast and sudden changes in the steering angle.

When the velocity of the vehicle is higher, the kinematic model loses its precision. This model does not include any dynamics behavior of the model. Therefore the vehicle yaw rate computation by this model is not precise at all at higher velocities.

On the other hand, the linearized constant velocity vehicle model provides data, which are close to the measured values. Some small and sudden changes

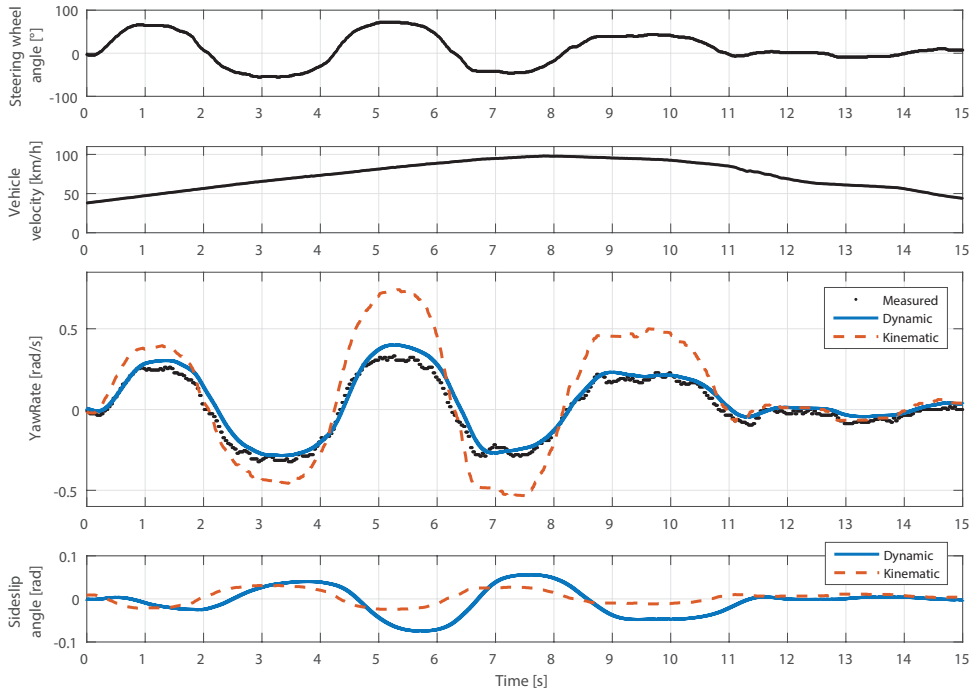

Figure 4.5: High-speed steering. Comparison of real measured values with simulated values. The data labelled 'Dynamic' represents the linear constant velocity vehicle model.

in the vehicle yaw rate caused by surface conditions are not precisely computed since the vehicle model has only the steering wheel angle and vehicle speed as the input. The gravel on one side of the airfield creates the difference of precision between left and right turn in figure 4.5. The tires were generating less side force when the vehicle was turning right which resulted in lower vehicle yaw rate.

Chapter 5

Torque vectoring control system

5.1 Introduction

The main idea of the torque vectoring described in the section 1.2 is to modify the vehicle dynamics. The goal is to eliminate oversteer or understeer in order to achieve neutral vehicle behavior and improve the vehicle stability. The torque vectoring controller designs described in this chapter serve as basic research in this area of vehicle dynamics. This work provides an elemental description of vehicle dynamics controllers together with a summary of the issues.

5.2 Feedforward control

Simple feedforward control system using the steering angle as input and the difference of the torques as the controlled variable is the first selected technique for controlling the vehicle yaw rate. The scheme of the feedforward torque vectoring controller is shown in figure 5.1.

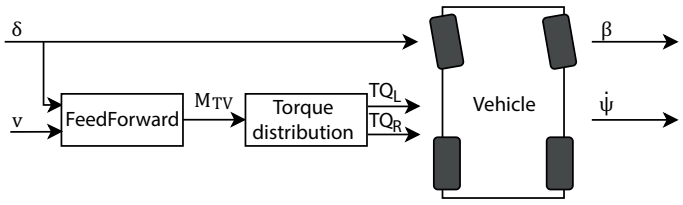

Figure 5.1: Feedforward torque difference controller. Scheme of simple feedforward controller with steering angle and vehicle velocity as input and torque difference as the controlled variable. The vehicle velocity input disables the controller for lower speeds.

The linearized constant velocity vehicle model (eq. 2.5.1) with the difference yaw moment as additional input can be used for studying the influence of developed feedforward controller on the vehicle dynamics.

The simple feedforward control law can be expressed as

$$M_{TV} = k \cdot \delta_w \cdot g(v), \tag{5.1}$$

where M_{TV} is the desired value of the vehicle yaw moment, k is the feedforward gain, δ_w is the steering wheel angle and the function $g(v)$ disables the torque vectoring for lower vehicle speeds.

The required torque difference for left and right wheel can be calculated as

$$\Delta TQ_L = -\frac{r}{2w} M_{TV} \qquad \texttt{and} \qquad \Delta TQ_R = \frac{r}{2w} M_{TV}, \tag{5.2}$$

where r is the rear wheel diameter and ΔTQ_L and ΔTQ_R are torque differences for left and right wheel respectively. The torque differences are then added to the required torque resulting in final equations

$$TQ_L = \frac{TQ_{req}}{2} - \frac{r\delta_w g(v)}{2w} k \qquad \texttt{and} \qquad TQ_R = \frac{TQ_{req}}{2} + \frac{r\delta_w g(v)}{2w} k, \tag{5.3}$$

where TQ_{req} is the required torque and TQ_L and TQ_R are requested torques from left and right motor respectively.

Putting equations 2.28 and 5.1 together results into the following linearized vehicle model with feedforward controller:

$$\begin{bmatrix} \dot{\beta} \\ \ddot{\psi} \end{bmatrix} = \begin{bmatrix} -\frac{C_{\alpha 0,F}+C_{\alpha 0,R}}{mv} & -\left(1 + \frac{C_{\alpha 0,F} l_f - C_{\alpha 0,R} l_r}{mv^2}\right) \\ -\frac{C_{\alpha 0,F} l_f - C_{\alpha 0,R} l_r}{I_z} & -\frac{C_{\alpha 0,F} l_f^2 + C_{\alpha 0,R} l_r^2}{I_z} \end{bmatrix} \begin{bmatrix} \beta \\ \dot{\psi} \end{bmatrix} + \begin{bmatrix} \frac{C_{\alpha 0,F}}{mv} \\ \frac{C_{\alpha 0,F} l_f}{I_z} + \frac{k C_{\delta_w}}{I_z} \end{bmatrix} \delta, \tag{5.4}$$

where the coefficient C_{δ_w} is an approximation of the inverse function converting the front wheel angle to the steering wheel angle (fig. 4.2). The torque vectoring dependency on the vehicle velocity is neglected in this equation.

The Simulink implementation of the feedforward controller is shown in figure 5.2. The required torque M_{TV} is saturated, and the requested torque TQ_L and TQ_R for each wheel are calculated from the required torque value. The required torque M_{TV} is set to 0 when the speed is less than some parameterizable value.

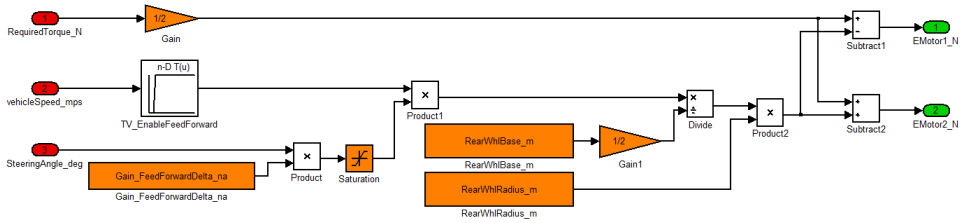

Figure 5.2: Torque vectoring feedforward algorithm. A simple implementation of feedforward controller using steering angle as input and torque difference as output. See experiment results in section 6.4.1.

5.3 Feedback control

The feedback control usually requires some reference value, which will be controlled by the controller. In our case, the controlled variable is the vehicle yaw rate. The driver's input is only the vehicle steering angle. The vehicle velocity is still assumed to be constant.

The parameterizable vehicle models can be used as a reference value generators enable to control and change the desired amount of the vehicle yaw rate. For example, the vehicle parameter for the vehicle weight in the models can be set to the lower value. Then the feedback control system algorithm affects the vehicle dynamics to match the real dynamics with the desired one. With this approach, the vehicle dynamics, stability and the driver's comfort can be improved.

5.3.1 Generator of reference values

In the section 4.4, the comparison between real vehicle data and the data simulated using the kinematic vehicle model and the linear constant velocity vehicle model was presented. These models provide the data, which can be used as a reference models with enough precision. In figure 5.3 the implementation of these models in Matlab Simulink is shown.

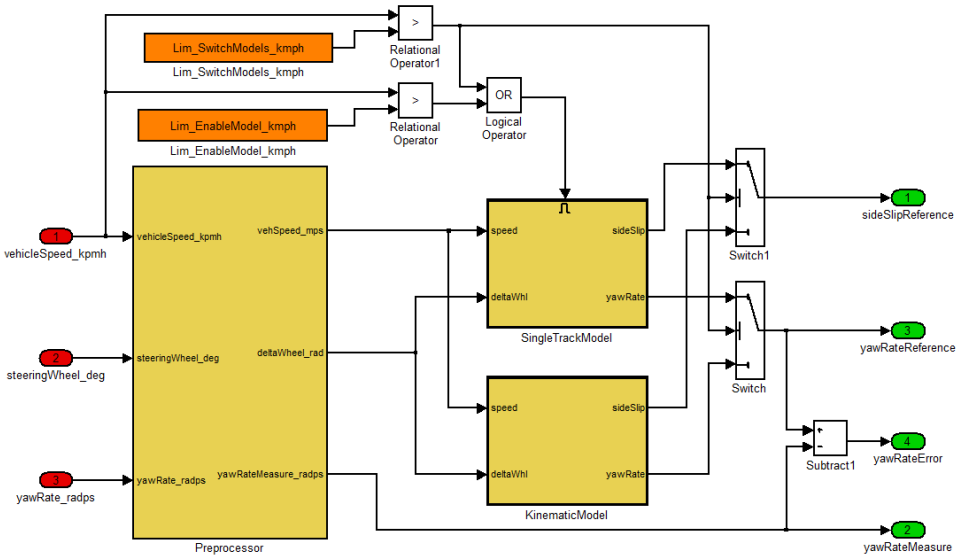

Figure 5.3: Vehicle models implementation. The implementation of the algorithm for switching between the kinematic and the linear constant velocity vehicle model in the Simulink scheme.

The first Simulink block in figure 5.3 after the inputs is the Preprocessor. This block prepares the values for the mathematical models and converts inputs to the right units - for example vehicle velocity is converted from $\mathrm{km\,h^{-1}}$ to $\mathrm{m\,s^{-1}}$ and the input steering wheel angle in degrees is converted to the front tire steering angle in radians used for the reference value computation (using static the characteristics in figure 4.2).

The reference value generator uses the kinematic vehicle model (eq. 2.3) for precise computation of vehicle states at the vehicle velocities close to zero. The linear constant velocity vehicle model (eq. 2.5) is then enabled for calculation when the vehicle velocity is higher than the parameterizable value `Lim_EnableModel_kmph`. Then if the vehicle velocity exceeds another parameterizable value `Lim_SwitchModels_kmph`, the kinematic vehicle model reference values are replaced with the linearized constant velocity vehicle model values. The actual velocity limit for the reference values switching has to be greater than the enabling velocity limit. It allows the internal integrator blocks to integrate value from their reset state correctly.

The generator also provides a calculation of error between the reference value of the vehicle yaw rate and the actual measured value.

5.3.2 Feedback control: yaw rate

One of the simple ways to control the reference variable is using a desired reference value, the value from the feedback and the proportional regulator to compute action M_{TV}. The scheme of this regulator is shown in figure 5.4.

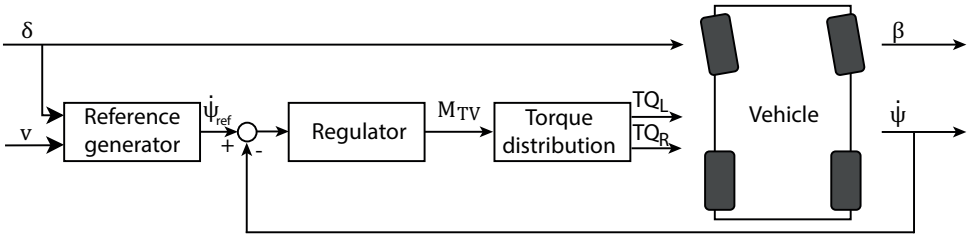

Figure 5.4: Feedback control - yaw rate. Scheme of simple feedback controller using generated yaw rate as the reference value.

The implementation of the used proportional controller is shown in figure 5.5. It was implemented as PID regulator with anti-windup for future purposes, but only the proportional part was used in the vehicle dynamics experiments. All regulator parameters are fully tunable. The desired value of the vehicle yaw moment can be computed using three parts of the PID regulator including the saturation and anti-windup algorithm, which can be turned off. Finally, the desired value of the vehicle moment is converted into the required torque for the left and right electric motor as it was in the feedforward controller.

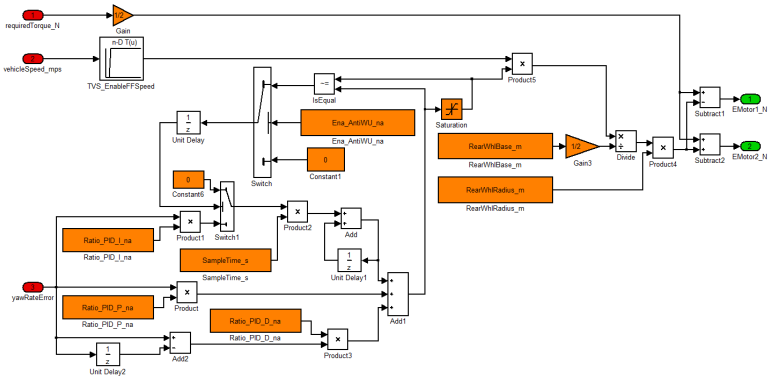

Figure 5.5: Torque vectoring proportional feedback regulator. The implementation of the used proportional feedback regulator using the generator of the vehicle yaw rate reference. See experiment results in section 6.4.2.

5.3.3 Feedback control: side acceleration

The motivation of this controller came from the weight transfer motion of the car. During the vehicle movement trough corner, the outer tires are

loaded more than the inner tires. Therefore they could transfer more torque to achieve more agile behavior of the vehicle. The controller scheme is shown in figure 5.6.

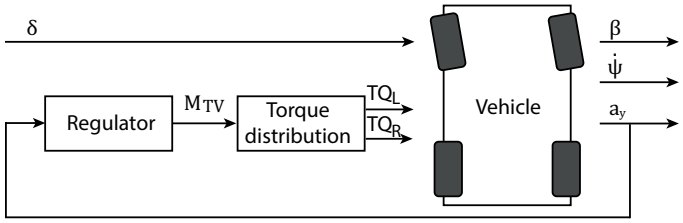

Figure 5.6: Feedback control - side acceleration. Scheme of simple the feedback controller.

The model-based software implementation of the feedback controller with the side acceleration is similar to the feedforward controller. However, the input to the controller is not the steering angle, but the measured side acceleration of the vehicle a_y. The implementation is shown in figure 5.7.

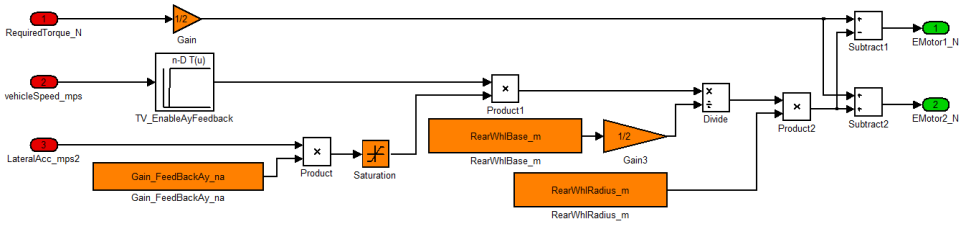

Figure 5.7: Torque vectoring feedback with side acceleration. The implementation of the feedback controller using side acceleration as input and torque difference as output. See experiment results in section 6.4.3.

5.4 Control systems target integration

The control systems described in this chapter were implemented using the model-based design software technique as the separate modules into a fully functional commercial automotive electric vehicle manager developed in the Porsche Engineering Services s.r.o.

The purpose of the torque vectoring module is to distribute required torque between the left and right electric motor in the test vehicle. The required torque is first computed by the driver's inputs from the throttle and also some higher instances of the control system such as derating systems based on the battery condition or temperature can adjust the required torque. An example of the functional cascade is shown in figure 5.8.

Completed control system software developed using Matlab Simulink and

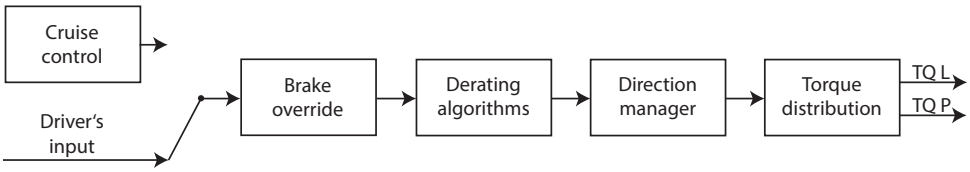

Figure 5.8: Vehicle control system. An example of the required torque calculation.

model-based development software design is converted into the C code using RealTime Workshop at the end. This code also includes the communication algorithms to read and write values to the CAN bus of the test vehicle.

Figure 5.9: ETAS ECU interface unit. The hardware interface used to flash the test vehicle target with the compiled control software.

The C code is then compiled into a file, which can be flashed into the vehicle controller memory using CAN and ETK bus. For this action professional software and hardware interface solutions by ETAS[1]were used (fig. 5.9). The target controller for this system is a standard automotive micro-controller placed directly inside the test vehicle. The test vehicle flashing procedure in progress is also shown in figure 4.1.

[1]ETAS GmbH. `www.etas.com`

Chapter 6

Experimental results

6.1 Introduction

This chapter dedicated to the torque vectoring experiments. The actuator authority tests answers the question about how much can the distribution of required torque between left and right wheel affect the vehicle handling. Then the experimental results from all implemented torque vectoring systems are compared and supplemented with opinions of the professional test driver.

6.2 Torque vectoring test maneuvers

The vehicle maneuver has to be chosen for the control systems evaluation. Different dynamics and statics tests are described in literature such as sweep steer test or step steer test. However, relatively big areas of clean tarmac are required for these experiments. Unfortunately, these areas are not available in the Czech Republic. Therefore, the double lane change vehicle test [17] standardized under ISO 3888-2 was chosen. The scheme of this test maneuver is shown in figure 6.1.

The double lane change vehicle maneuver consists of three segments. First is the entry segment with the length of 12 m and the width of this segment depends on the width of the test vehicle (1.1x vehicle width + 0.25 m). The second part is the sideline segment with the length of 11 m and the width of this segment also depends on the width of the test vehicle (vehicle width + 1 m). This segment has lateral offset equal to 1 m as seen in figure 6.1. The spacing between the entry segment and sideline segment is equal to 13.5 m. Finally, the exit segment is 12 m long and 3 m wide and the spacing between

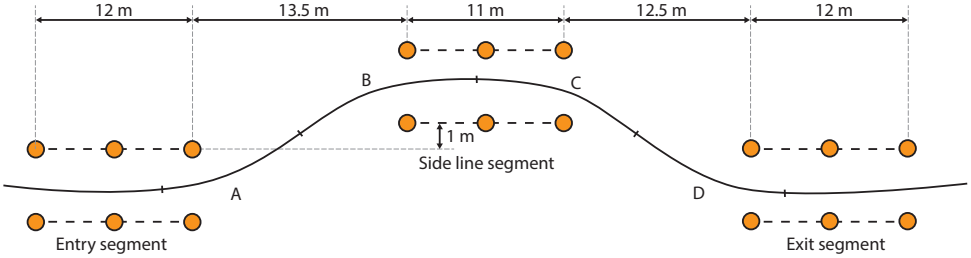

Figure 6.1: Double lane change test, ISO 3888-2. The maneuver was for better orientation separated into four turns. The black line is an example of the vehicle center of gravity movement.

sideline segment and exit segment is equal to 12.5 m.

For purposes of this thesis and more straightforward description of the maneuver, the double lane change test was separated into four different turns. The turn A and D are left turns, the turn B and C are right turns (see fig. 6.1). This separation helps later in this chapter to evaluate the actuator authority and experimental results of introduced torque vectoring control systems.

Each experiment was repeated several times, and the best results were chosen to eliminate human influence of the driver. The double lane change test is passed if no cone was knocked down. The vehicle dynamics experiments were performed with active cruise control set to 70 $\mathrm{km\,h^{-1}}$ on private airfield closed to the public.

6.3 Torque vectoring actuator authority experiments

The effects of the distribution of the required torque between left and right electric motor are usually known. However, the amount of influence to the actual dynamic vehicle behavior is typically unknown, so the in-depth view brings some benefits.

The implementation of the torque distribution system in the test vehicle was very simple before the work on this thesis began. Total required amount of torque was divided by two, and resulting value was sent to each motor. Within this chapter, this distribution will be called 50/50 distribution.

The influence of the non-equal distributions to the vehicle yaw rate is shown and analyzed in this section. Three different distributions were chosen - 40/60, 25/75 and 10/90 for the purposes of the analysis. Important notice has to be added to these numbers: the numbers represent the percentage of

total required torque, which is then requested by the electric motors. The lower number represents the amount of torque on the electric motor of the inner wheel, and the higher number represents the amount of torque on the electric motor if the outer wheel.

Therefore the switching of the signals depends on the sign of steering angle. Small dead-band zone together with simple hysteresis was implemented to smoother transitions of requested torques between right and left turns. An example of 25/75 torque distribution rates is shown in table 6.1. The implementation of this algorithm is shown in figure 6.2.

	$\delta > 20°$	$20° \geq \delta \geq -20°$	$-20° > \delta$
Left motor	25 %	50 %	75 %
Right motor	75 %	50 %	25 %

Table 6.1: Torque distribution rates. An example of 25/75 torque distribution between left and right electric motor. The positive steering angle generates positive[1]yaw rate.

The torque vectoring system had to satisfy basic safety rules such as direction (forward, reverse) control and the brake override. The software version of the developed module contained an algorithm for the feasibility of the torque vectoring actuator authority tests (see section 6.3). The Simulink scheme of this algorithm is in figure 6.2.

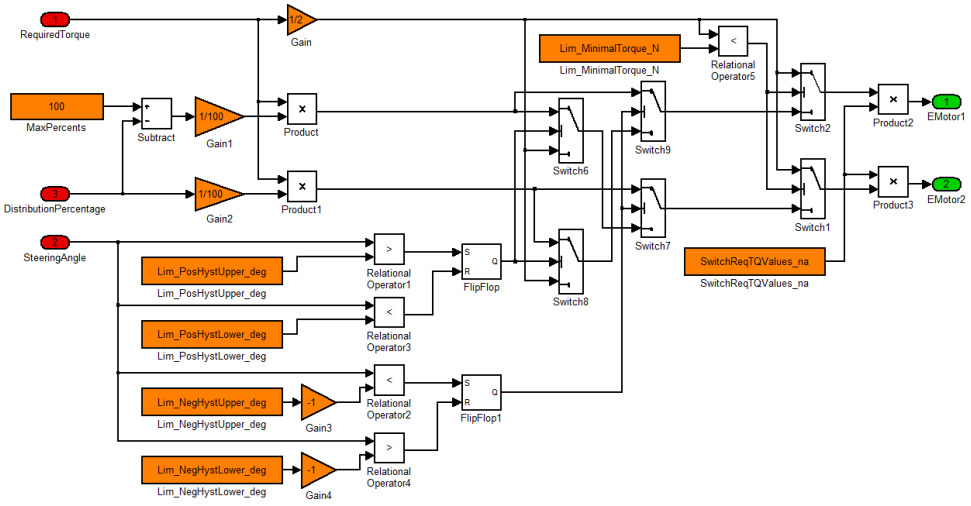

Figure 6.2: Torque vectoring actuator authority algorithm. A simple implementation of dead-band and hysteresis for the feasibility of the vehicle tests. See experiment results in section 6.3.

The required torque from the driver is after processing with derating algorithms divided based on the value of input signal `DistributionPercentage`.

[1]The positive yaw rate means left turn in the conventions of this diploma thesis.

This signal is taken directly from the vehicle CAN bus and can be modified online using simple slider application in connected PC. The series of switches then select the right value for each electric motor based on an actual position of the steering wheel. Finally, the requested torque is distributed only when positive torque is required so the forward direction mode of the vehicle is selected. The torque is distributed equally if the recuperation or breaking command occur.

The experimental results are shown in figure 6.3. The side acceleration and the yaw rate does not show significant change. Small differences in the figures can be explained by human factor. On the other hand, the steering angle shows significant improvements. If we compare the original 50/50 distribution with the 40/60 or 25/75, the driver's reactions and input steering angle are smoother, and the maximal steering angle amplitude is lower.

The amplitude of the steering angle is also lower if we look at the distribution 10/90. However, in this case, the vehicle dynamics react too much to the driver's input so he is forced to stabilize it. This situation can be seen between 2 and 2.6 seconds in figure 6.3.

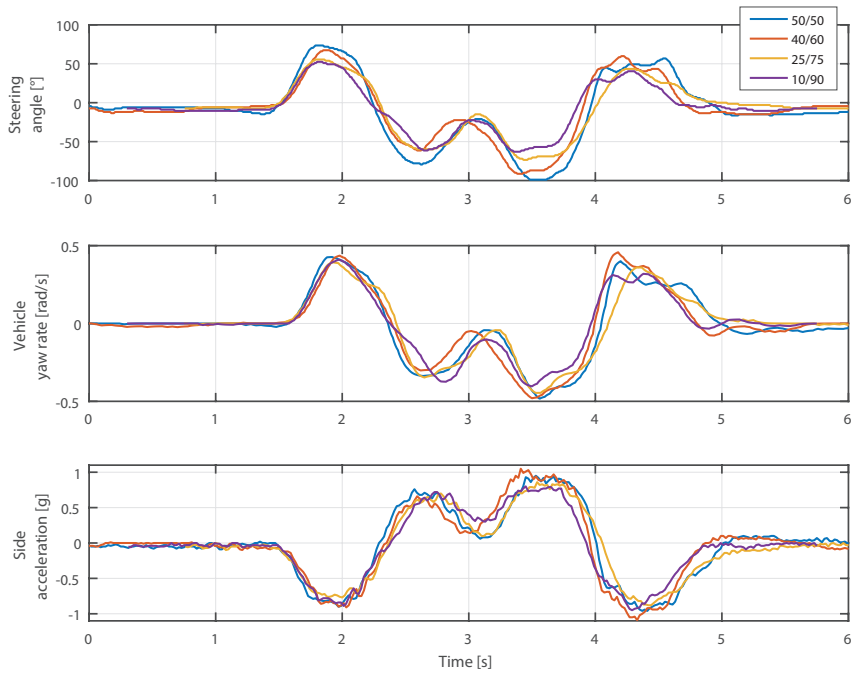

Figure 6.3: Torque vectoring actuator authority test. Double line change maneuver with different torque distribution settings.

The overall steering improvement is shown in figure 6.4. The bar graphs show the average steering angle during each turn labeled A, B, C and D together with the maximal amplitudes, which are displayed as a circles above the bars.

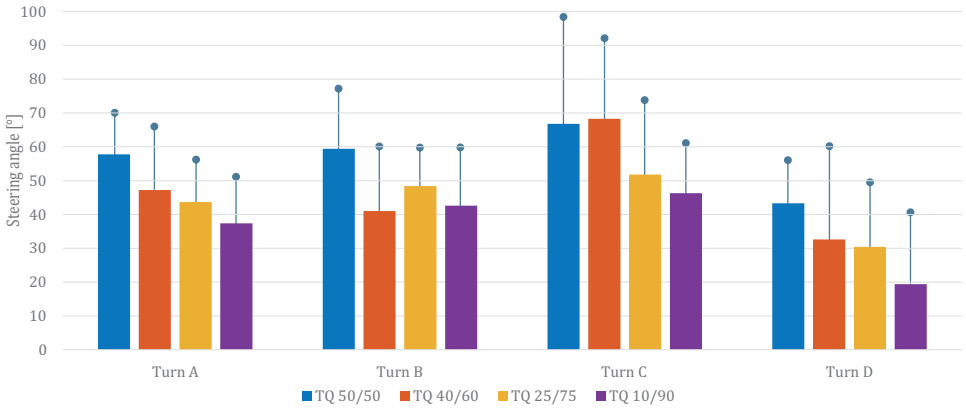

Figure 6.4: Torque vectoring actuator authority test, steering. Comparison of an average and maximum amplitude of the steering angle during the double line change maneuver with different torque distribution settings.

The decrease of the maximal amplitude of steering angle required for the particular maneuver together with the increased response of the vehicle dynamics to the driver's inputs can lead to an improvement of vehicle cornering.

6.4 Experimental results of torque vectoring systems

Each of the control systems presented in chapter 5 was tested on the test vehicle (figure 4.1). Several attempts of double lane change maneuver (section 6.2) with different settings were performed, evaluated and compared with the original algorithm without the torque vectoring. Each of the selected controller settings is provided with the commentary and vehicle behavior description from an experienced driver.

The test vehicle used for the test maneuvers in the default settings without the torque vectoring controller has action dynamics. The vehicle shows significant under-steer behavior. Therefore the driver must show some effort to pass the double lane change test correctly.

6.4.1 Results of feedforward control

The results of the double lane change maneuvers with the feedforward controller (section 5.2) with different settings are shown in figure 6.5. The feedforward gain was set to values 0, 1, 1.5 and 2 for each attempt.

Comparing the vehicle yaw rate and side acceleration shows no particular difference in the shapes of the curves. Small changes and variations are influenced by test driver error and repetition of the tests.

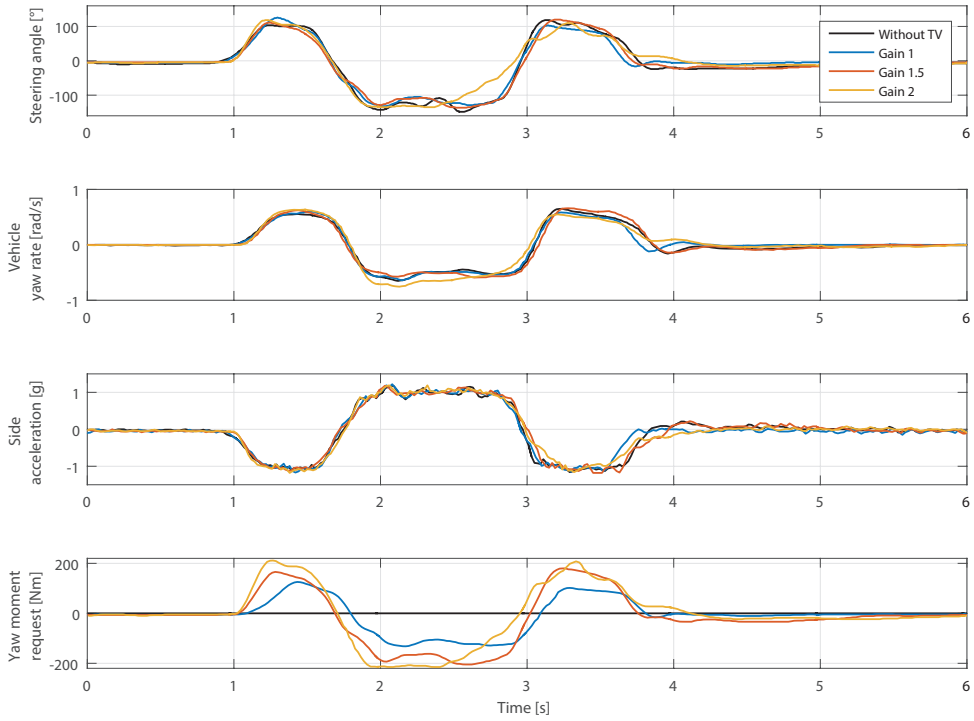

Figure 6.5: Feedforward regulator, test results.

1. **Feedforward gain 1:** The steering angle with this setting is smoother than during the default maneuver mainly in section B, C, and D.

   According to the driver's description, the vehicle has less understeer behavior than in the default case. It is closer to the neutral vehicle behavior. The controller intervention to the vehicle dynamics is noticeable.

2. **Feedforward gain 1.5:** The test vehicle with this setting of the feedforward controller shows a slightly oversteering property according to the driver, but most of the time the vehicle dynamics remain controllable.

   The steering angle shows improvement along the whole duration of the maneuver. The shape is smoother than in the previous test. On the other hand, the driver had to slightly stabilize the car movement.

3. **Feedforward gain 2:** In this case, the vehicle showed unwanted oversteer properties. Although the test vehicle passed the double-line change test, the driver had to make a significant effort to complete the maneuver with success.

A better comparison of the results of each test maneuver is shown in figure 6.6, where vehicle side-slip angle is estimated using Kalman filter observer.

The maneuver without torque vectoring has a slightly higher side-slip angle with big disturbances between 2 and 3 seconds.

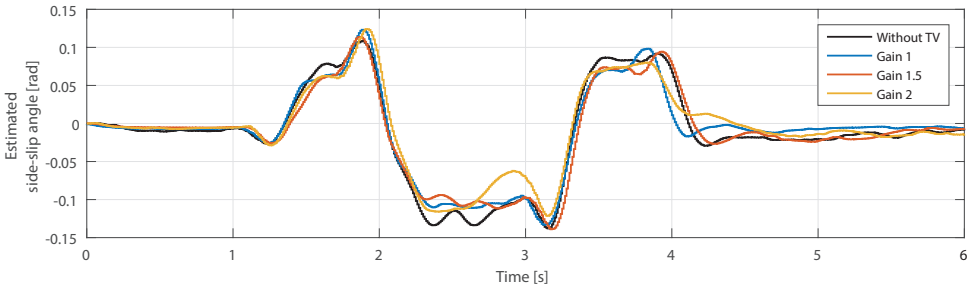

Figure 6.6: Feedforward regulator, side-slip. Comparison of estimated side-slip angle.

The first two controlled maneuvers show improvement of the vehicle handling and much steadier curve, mainly during the B and C section of the maneuver. On the other hand, the third experiment confirms the driver's effort to keep vehicle stable in the desired direction.

Figure 6.7 shows simulated Bode characteristics of the vehicle model with varying feedforward gain. The resulting characteristics correspond with the observed results of the feedforward. Increased yaw rate gain should result in faster vehicle dynamics response.

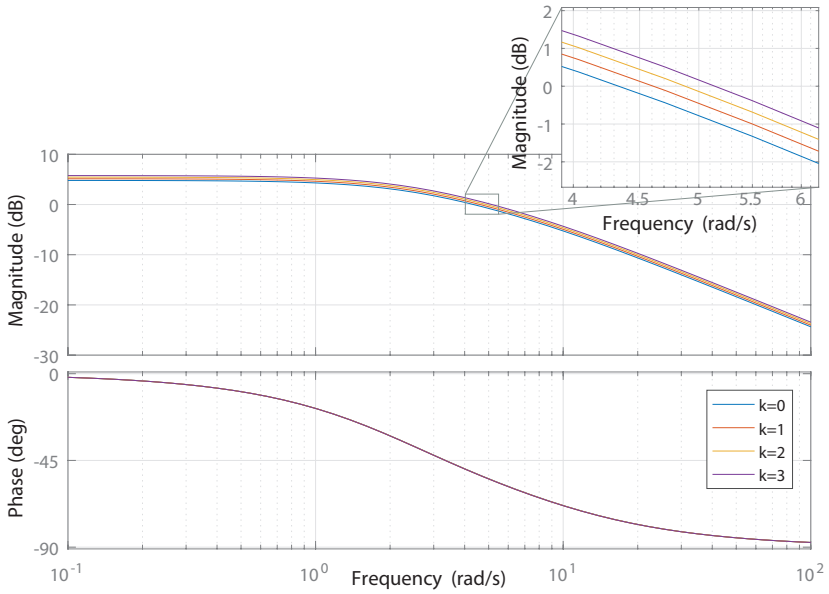

Figure 6.7: Bode characteristics of the feedforward torque difference controller. As the feedforward gain increases, the frequency gain is also increased.

6.4.2 Results of feedback control: yaw rate

Only the proportional part of the PID controller (section 5.3.2) together with the reference yaw rate generator was used to control the vehicle dynamics. The changes in the vehicle states are rapid for an integral part. Therefore the integral gain was set to 0. Also, the derivative gain was set to 0 to reduce the error caused by low-resolution measurement of the yaw rate sensor placed directly inside the vehicle. The proportional gain was set to values 0, 500, 1000 and 1500.

The comparison of the vehicle yaw rate and side acceleration shows a more significant difference between each controller settings. However, small changes and variations could be caused by the difference of test driver's input.

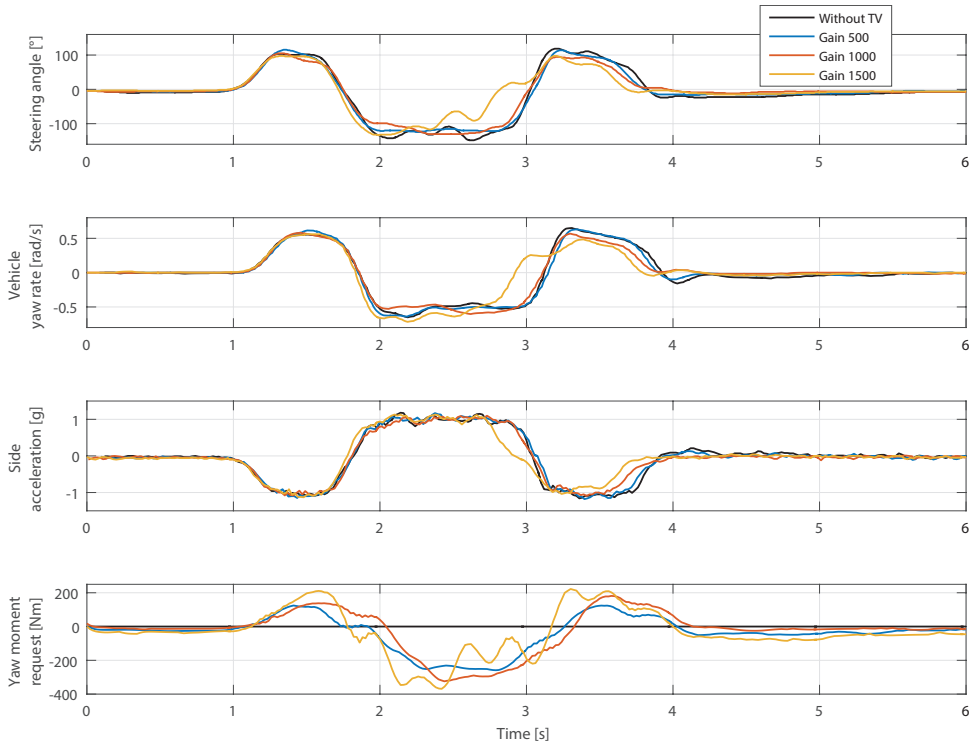

Figure 6.8: Feedback regulator test results.

1. **Proportional gain 500:** The steering angle with this setting of the feedback controller does not show any difference compared to the default test experiment. The vehicle yaw rate and side acceleration are similar to the default values.

   On the other hand, the vehicle has improved handling according to the driver. The vehicle has less understeer behavior and vehicle dynamic was slightly improved.

2. **Proportional gain 1000:** The improvement in the smoothness of the steering angle can be seen along the whole duration of the maneuver. The vehicle response to the driver's actions was improved, and the vehicle had no more understeer behavior.

3. **Proportional gain 1500:** In the last case of the feedback controller settings, the vehicle behavior was very poor with huge oversteer behavior. The driver had to stabilize the vehicle dynamics to safely complete the maneuver. His stabilizing action is nicely seen in the steering angle figure (figure 6.8) between 2.5 and 3 seconds.

The comparison of the results of each test maneuver is shown in figure 6.6, where vehicle side-slip angle is estimated using Kalman filter observer. The maneuver without torque vectoring has a slightly higher side-slip angle with significant disturbances between 2 and 3 seconds.

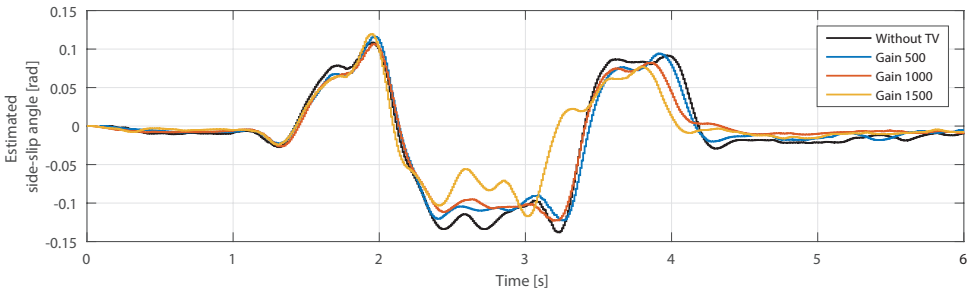

Figure 6.9: Feedback regulator test results. Comparison of estimated side-slip angle.

The first settings of the feedback regulator showed improvement in the vehicle behavior, but the measured results were nearly the same compared to the default experiment. If we look at the estimated side-slip comparison, the difference can be immediately seen. The shape of the estimated slip-angle is smoother, and the values are lower.

Nearly the same shape of the side-slip angle values applies for the second run. For the third test series, the instability of the vehicle (between 2.5 and 3 seconds) together with the oversteer behavior (between 3 and 3.5 seconds) can be seen in figure 6.9.

6.4.3 Results of feedback control: side acceleration

Finally, the results of the third torque vectoring controller - feedback with the side acceleration - are shown in figure 6.10.

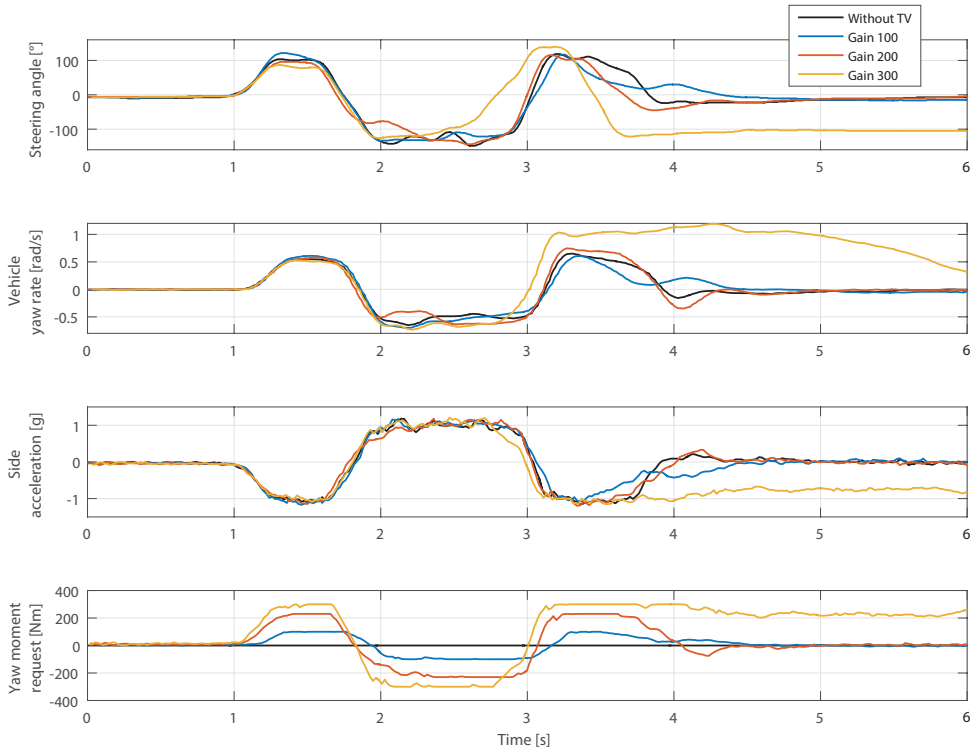

Figure 6.10: The test results of the regulator with side acceleration.

1. **Gain 100:** The input steering angle curve was smooth. The vehicle dynamics was improved, but still with understeer behavior. The influence of the controller was noticeable by the driver.

2. **Gain 200:** This controller settings provided the best vehicle behavior among all tested controllers. The test vehicle had neutral behavior, the movement during the maneuver was smooth, only with small disturbances. The influence of the controller was noticeable.

3. **Gain 300:** This controller setting was probably the worst. The vehicle had big over-steer behavior. During the transition between section B and C of the double line change maneuver the vehicle lost traction of the front tires. The driver tried to compensate by quick steering action, which helped to pass the section C into the section D.

   However, in the middle of the section D, the vehicle lost traction completely. The driver tried to stabilize the vehicle, the steering angle was at 100 degrees, but the vehicle continued spinning in the skid. In this case, the vehicle did not pass the double line change test.

   The feedback controller design with side acceleration did not helped during the vehicle skid. The vehicle was spinning, and the side acceleration was still high. That resulted in additional yaw moment request, which worsened the situation.

Finally, the comparison of the estimated side-slip angle during the maneuver is shown in figure 6.11. First two settings of the controller show small improvements mainly in the section D of the maneuver. The third controller settings show the skid of the vehicle during the D section of the double line change maneuver.

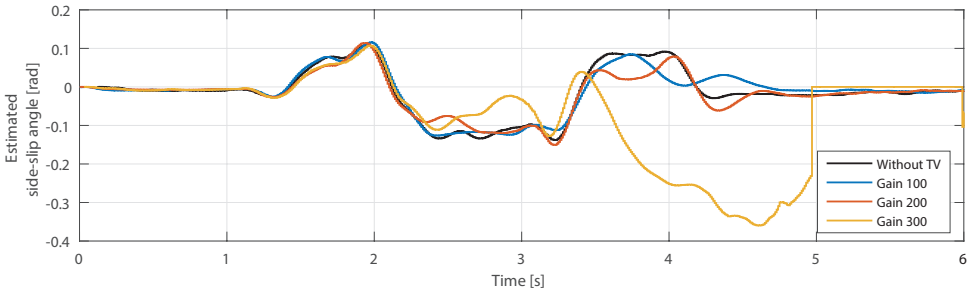

Figure 6.11: Side acceleration regulator, side-slip results. Comparison of estimated side-slip angle.

Chapter 7

Results

The results of this thesis can be summarized as follows:

- **Vehicle models** - three vehicle models (kinematic model, single-track model and linearized constant speed model) were described and evaluated.
- **Linear analysis** - the linearized constant speed vehicle model was analyzed in depth. Each parameter value of the vehicle was varied within a reasonable range, and the influence on the model dynamics and output responses was compared and described.
- **Experimental identification** - the parameters of the vehicle were measured or experimentally identified. The values were validated by simple experiments with the test vehicle.
- **Control architecture** - various torque vectoring control algorithms using feedforward and feedback were developed and integrated into a fully functional electric vehicle control system. The algorithms were implemented using model-based software design and compiled using professional automotive production framework.
- **Vehicle experimental tests** - two vehicle dynamics tests were realized on the closed airfield. Developed feedback and feedforward controllers were tested by an experienced driver.
- **Documentation of results** - all vehicle dynamics test results were analyzed, described and evaluated. The change of the vehicle behavior was described by an experienced driver.

Chapter 8

Conclusions and future work

The vehicle dynamics can be described in various ways. Kinematic vehicle model provides perfect estimation of the vehicle states at lower vehicle velocities. However, as the vehicle speed increases, this model loses its precision. On the other hand, the single track vehicle model with the linearized version provides a good result at higher vehicle velocities.

Most significant parameters of the vehicle models are the front and the rear tire slip coefficients. The measurement of these coefficients is problematic. Therefore, they have to be estimated using, for example, Kalman filters or by fitting these parameter by an experimental identification.

The torque vectoring control system can improve the vehicle dynamics and handling. The lateral vehicle behavior can be stabilized or more excited depending on the chosen control strategy. The best outcome in agilization of the vehicle produces the simple feedforward controller as the results showed. On the other hand, the desired value generator together with the feedback controller provides more options to control and adjust the vehicle dynamics in various conditions. However, the lateral vehicle control using only yaw rate as reference variable is usable only in excellent weather conditions and during some maneuvers.

This work can be used as a fundamental source of information about the vehicle dynamics, lateral control and the vehicle reaction to the different torque distribution. Follow-up work can use the established framework and improve presented control systems by including the vehicle side-slip estimation and control. Also, the advanced optimal and robust controllers can be developed after gathering the appropriate control constraints.

Appendix A

Bibliography

[1] Dr. Ing. h.c. F. Porsche AG. SPECIFICATIONS 2007 PORSCHE® Boxster & Boxster S. [online], Cited 9. 1. 2018.

[2] J. Ghosh, A. Tonoli, and N. Amati. A torque vectoring strategy for improving the performance of a rear wheel drive electric vehicle. In *2015 IEEE Vehicle Power and Propulsion Conference (VPPC)*, pages 1–6, Oct 2015.

[3] M. Guiggiani. *The science of vehicle dynamics: handling, braking, and ride of road and race cars*. Springer, Dordrecht, 2014.

[4] L. Hafner. *Real-time tire models for lateral vehicle state estimation*. PhD thesis, Technischen Universität Wien, Fakultät für Maschninenbau, Wien, 2008.

[5] R. N. Jazar. *Vehicle dynamics: theory and application*. Springer, New York, 2nd edition, 2014.

[6] G. Kaiser, F. Holzmann, B. Chretien, M. Korte, and H. Werner. Torque vectoring with a feedback and feed forward controller - applied to a through the road hybrid electric vehicle. In *2011 IEEE Intelligent Vehicles Symposium (IV)*, pages 448–453, June 2011.

[7] G. Kaiser, Q. Liu, C. Hoffmann, M. Korte, and H. Werner. Torque vectoring for an electric vehicle using an lpv drive controller and a torque and slip limiter. In *2012 IEEE 51st IEEE Conference on Decision and Control (CDC)*, pages 5016–5021, Dec 2012.

[8] D. Karnopp. *Vehicle stability*, volume 171. Dekker, New York, 2004.

[9] J. Kong, M. Pfeiffer, G. Schildbach, and F. Borrelli. Kinematic and dynamic vehicle models for autonomous driving control design. In *2015 IEEE Intelligent Vehicles Symposium (IV)*, pages 1094–1099, June 2015.

[10] Z. Luan and Z. Wu. Research on lateral dynamics of distributed driving vehicle with torque vectoring steering. In *2015 IEEE International Conference on Mechatronics and Automation (ICMA)*, pages 308–312, Aug 2015.

[11] G. Mastinu and M. Plöchl. *Road and off-road vehicle system dynamics handbook*. CRC Press, Boca Raton, 2014.

[12] M. Mondek and M. Hromčík. Linear analysis of lateral vehicle dynamics. In *2017 21st International Conference on Process Control (PC)*, pages 240–246, June 2017.

[13] H. B. Pacejka. *Tyre and vehicle dynamics*. Butterworth-Heinemann, Oxford, 1st edition, 2002.

[14] R. Rajamani. *Vehicle Dynamics and Control*. Rajesh Rajamani, 2006.

[15] V. Scheuch, G. Kaiser, M. Korte, P. Grabs, F. Kreft, and F. Holzmann. A safe torque vectoring function for an electric vehicle. In *2013 World Electric Vehicle Symposium and Exhibition (EVS27)*, pages 1–10, Nov 2013.

[16] G. Vandi, D. Moro, F. Ponti, R. Parenti, and G. Einaudi. Vehicle dynamics modeling for real-time simulation. In *SAE Technical Paper*. SAE International, 09 2013.

[17] VEHICO. ISO lane change test. [online], Cited 9. 1. 2018.

[18] F. Vlk. *Dynamika motorových vozidel: jízdní odpory : hnací charakteristika : brzdění : odpružení : řiditelnost : ovladatelnost : stabilita*. Nakladatelství a vydavatelství Vlk, Brno, 1. vyd. edition, 2000.

[19] A. v. Zanten. *Regulace jízdní dynamiky: jízdní bezpečnost motorových vozidel*. Robert Bosch, Praha, 1. české vyd. edition, 2001.

Appendix B

List of abbreviations

ABS Anti-lock braking system

CAN Controller area network

CG Center of gravity

ECU Electronic control unit

ESP Electronic stability program

PC Personal computer

TV Torque vectoring

Appendix C

List of symbols

a	acceleration
α	tire side-slip angle
β	vehicle side-slip angle
C_α	tire cornering stiffness factor
δ	wheel angle
f	front track
F_x	longitudinal force
F_y	lateral force
F_z	normal load
I_z	moment of inertia about the z-axis
l	lenght of the vehicle
m	vehcile weight
μ	friction coefficient
r	vehicle tire diameter
R	cornering radius
TQ_R	right motor torque
TQ_L	left motor torque
v_x	longitudinal velocity
v_y	lateral velocity

w rear track

ψ vehicle yaw

$\dot{\psi}$ vehicle yaw rate